Phase-sensitive modulation instability in asymmetric coupled quantum wells

Rohit Mukherjee [1,*] S. Konar [1] and Puspashree Mishra [2]
[1]*Department of Physics, Birla Institute of Technology, Mesra, Ranchi, Jharkhand 835215, India*
[2]*Solid State Physics Laboratory, DRDO, Lucknow Road, Timarpur, Delhi 110 054, India*

(Received 18 November 2020; accepted 11 March 2021; published 22 March 2021)

This paper presents a theoretical investigation of the phase-sensitive modulation instability of a continuous or quasicontinuous probe beam in an asymmetric coupled quantum well (ACQW) system facilitated by electromagnetically induced transparency. The dispersive properties of the probe beam can be controlled not only by the Rabi frequency of the control field but by the relative phase between them as well. The ACQW system exhibits large Kerr and quintic nonlinearities which could be controlled by controlling the relative phase of the probe beam. The probe beam is modulation unstable, and the gain and the bandwidth of unstable frequencies could be controlled by the phase of the probe beam. The gain of the instability disappears at certain values of phase and at certain other values of the phase the gain of the instability, and the bandwidth of unstable frequencies could be made large. Similarly, at certain values of the probe phase, the interplay of fourth-order dispersion and nonlinearity leads to the creation of discrete sidebands of the modulation instability. Both the fourth-order dispersion and quintic nonlinearity considerably reduces the growth and bandwidth of unstable frequencies.

DOI: 10.1103/PhysRevA.103.033517

I. INTRODUCTION

During past two decades, the phenomena of quantum coherence and interference effects in semiconductor nanostructures have received tremendous attention due to important applications in telecommunications and signal processing [1–4]. Some of these quantum coherent processes are lasing without inversion [5], coherent population trapping [6], electromagnetically induced transparency (EIT) [7,8], giant Kerr nonlinearity [9], four-wave mixing (FWM) [4], optical bistability [10,11], subluminal and superluminal light propagation [12–14], soliton generation [13], etc., have been investigated both theoretically as well as experimentally. The EIT phenomenon is the result of interference between quantum states that is facilitated by external electromagnetic fields leading to the transparency in an initially opaque medium [8]. The EIT can be used to manipulate group velocity of light pulses in dispersive media and enhance nonlinear optical processes [15,16]. It can minimize linear and two-photon absorption, and can enhance Kerr as well as quintic nonlinearities [7,9,17–19].

Optical materials exhibiting large nonlinearity have received considerable attention due to potential applications since large nonlinearities ensure operation of the device at low light power [9,19,20–22]. The existence of large Kerr nonlinearity in semiconductor quantum wells (SQWs) under the regime of EIT has been known for some time [23–25], while the existence of enhanced quintic nonlinearity has been predicted very recently [14,26–28]. Materials that exhibit significant quintic nonlinearity play an important role in quantum information processing such as quantum memory of light [3,4], three-qubit quantum processing [1,29], generation of correlated photon pairs [4], etc. Furthermore, quintic nonlinearity reduces the phase noise, thereby improving the performance of interferometry [30], and consequently, it can improve the high-precession measurements [31]. Materials exhibiting significant quintic nonlinearity can produce new phenomena such as liquid light condensates [32], stable two-dimensional (2D) soliton formation, as well as bistable solitons [33]. Recently it was realized that the phase of the interacting optical fields in a close-loop interaction scheme may provide necessary control over several interesting properties in semiconductor quantum well and atomic systems [34–39]. For example, electron population, absorption and dispersion properties, electromagnetically induced transparency [34,35], subluminal and superluminal light propagation [36], optical bistability (OB) and multistability [37], Kerr nonlinearity [38] in semiconductor quantum wells, as well as subwavelength atom localization [39] in atomic media can be controlled by suitably choosing the phase of the interacting optical beams or pulses. Borgohain *et al*. [25] have examined modulation instability in a three-level symmetric quantum well system by incorporating higher-order nonlinearity and dispersion. Roles of quintic nonlinearity and the effect of control detuning were examined. However, the role of the phase of the probe beam in determining the dynamics of the modulation instability (MI) has failed to draw desired attention. Recently it was realized that the phase of the interacting optical fields may play important role in determining the dynamics of several important phenomena; therefore it shall be pertinent to know the role of phase of the probe beam in the dynamics of MI. In view of the above, the primary aim of the present investigation is to explore the role of the phase of the probe beam in determining its nonlinear dynamics, in particular, modulation instability. Thus we plan to examine the phase control MI of a

*phdap10002.18@bitmesra.ac.in

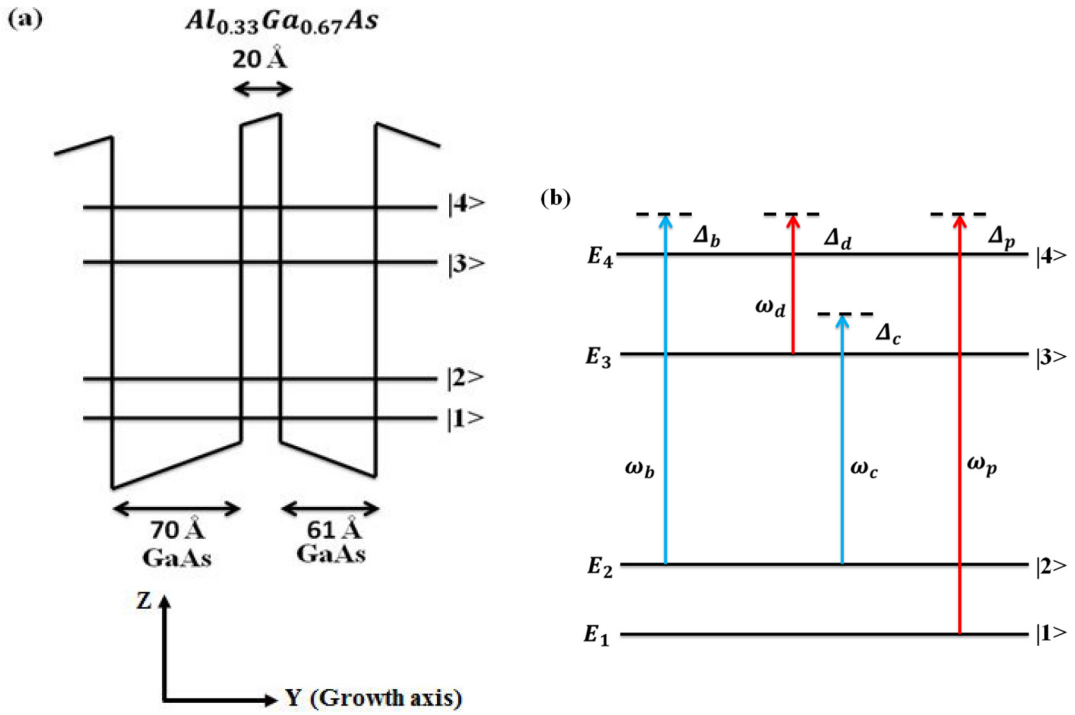

FIG. 1. (a) Schematic diagram of a single-period asymmetric double quantum well which consists of two thick GaAs wells having thickness 70 and 61 Å, respectively, and separated by a 20-Å thin $Al_{0.33}Ga_{0.77}As$ barrier. (b) Excitation scheme.

continuous or quasicontinuous optical probe beam in an asymmetric coupled quantum well (ACQW) system facilitated by electromagnetically induced transparency.

The rest of the article is organized as follows: In Sec. II we present the theoretical model of an array of asymmetric coupled quantum wells interacting with one probe and three control laser fields. In this section we also derive the analytical expressions of susceptibilities of the probe beam. The properties of phase-controlled linear, Kerr, and quintic nonlinearities are examined in Sec. III. In Sec. IV we derive the phase-induced dispersion parameters and nonlinear Schrödinger equation of the propagating probe. In Sec. V we investigate the MI of the continuous or quasicontinuous probe field and examine how the growth rate of the instability is affected by the variation of relative phase between the applied fields. Finally, an abridged conclusion is included in Sec. VI.

II. THEORETICAL MODEL AND GOVERNING EQUATIONS

To begin with, we consider an array of 50 modulation-doped ACQWs, which is grown on a semi-insulating GaAs substrate. A single period of the coupled well and the corresponding excitation scheme are depicted in Fig. 1. Each period of the ACQW consists of two thick GaAs wells of thickness 61 and 70 Å, respectively, separated by a 20-Å thin $Al_{0.33}Ga_{0.77}As$ barrier. Each coupled quantum well period is separated by a barrier of $Al_{0.33}Ga_{0.77}As$ of thickness 950 Å, and the structure is very much similar to that reported in Ref. [40]. The two wells in the asymmetric coupled quantum wells (ACQW) are strongly coupled due to the small separation between them, and hence, electronic wave functions of the coupled system overlap. These wave functions and corresponding energy levels depend on the width, depth, as well as separation between these wells. The electronic energy levels and corresponding wave functions could be computed by solving self-consistently the Schrödinger and Poisson's equations in the envelope function formalism [41]. The ACQW system considered in the present study has been intensely used to investigate propagation of solitons and other phenomena [42,43]. Since the computed energy levels are available elsewhere [40], we pick up the values, and interested readers are referred to Ref. [40]. Note that since the thickness of the quantum wells determines the value of the energy levels, the susceptibilities of the probe field which shall be derived in this section shall not explicitly depend on the thickness of the quantum wells. The energy values of different subbands of the coupled quantum wells are 66, 81, 201, and 250 meV, respectively. In the present investigation we assume that the doping concentration in the coupled quantum well is low such that electron-electron interaction produces negligible influence. As a result, many-body effects arising from electron-electron interactions are not considered in the present investigation. The quantum well system interacts with one continuous wave (CW) or quasicontinuous probe field of amplitude E_p with angular frequency ω_p, and three control laser fields of amplitudes E_c, E_d, and E_b with angular frequencies ω_c, ω_d, and ω_b, respectively. The probe field acts on the transition from $|1\rangle$ to $|4\rangle$, while the three control fields act on the transitions from $|2\rangle$ to $|3\rangle$, $|3\rangle$ to $|4\rangle$, and $|2\rangle$ to $|4\rangle$, respectively. In the present system all the lights propagate along the z axis within the ACQW sample. We consider a transverse magnetic polarized probe, since the dipole operator for intersubband transitions is polarized along the growth axis.

Electric fields which are interacting inside the ACQW can be written as

$$\vec{E} = \sum_{j=p,c,d,b} \hat{e}_j E_j e^{i(k_j z-\omega_j t)} + \text{c.c.}, \tag{1}$$

where $\hat{e_p}$, $\hat{e_c}$, $\hat{e_d}$, and $\hat{e_b}$ are, respectively, the unit vectors along the polarization direction of the probe and control fields. Here k_j $(j = p, c, d, b)$ is the corresponding wave vector of the applied field, and the subscripts p, c, d, and b signify the probe, first, second, and third control field, respectively, while the term c.c. signifies the complex conjugate. By adopting the rotating wave approximation (RWA) [44], the semiclassical Hamiltonian of the coupled quantum well system can be written as

$$\hat{H} = \hat{H}_0 + \hat{H}_{\text{int}}, \tag{2}$$

where

$$\hat{H}_0 = \sum_{j=1}^{4} E_j |j\rangle\langle j|, \tag{3}$$

and

$$\begin{aligned}\hat{H}_{\text{int}} = &-\hbar[\Omega_p e^{i(k_p z-\omega_p t)}|4\rangle\langle 1| + \Omega_c e^{i(k_c z-\omega_c t)}|3\rangle\langle 2| \\ &+ \Omega_d e^{i(k_d z-\omega_d t)}|4\rangle\langle 3| \\ &+ \Omega_b e^{i(k_b z-\omega_b t)}|4\rangle\langle 2| + \text{H.c.}].\end{aligned} \tag{4}$$

Here $\hat{H}_0$ represents the unperturbed Hamiltonian of the system in the absence of applied fields, and $\hat{H}_{\text{int}}$ signifies the interaction of the electrons of the coupled quantum well with the electromagnetic fields. Due to the close-loop configuration, the properties of the semiconductor quantum well (QW) are quite sensitive to the phases of the applied fields; therefore the phases of the corresponding electromagnetic fields have been appropriately taken into account in the intersubband transition (ISBT) Rabi frequencies of the probe (Ω_p) and control fields $(\Omega_c, \Omega_d, \Omega_b)$, which are defined as $\Omega_p = |\Omega_p|e^{-i\phi_p} = \frac{\hat{\mu}_{41}\hat{e_p}E_p}{\hbar}e^{-i\phi_p}$, $\Omega_c = |\Omega_c|e^{-i\phi_c} = \frac{\hat{\mu}_{32}\hat{e_c}E_c}{\hbar}e^{-i\phi_c}$, $\Omega_d = |\Omega_d|e^{-i\phi_d} = \frac{\hat{\mu}_{43}\hat{e_d}E_d}{\hbar}e^{-i\phi_d}$, and $\Omega_b = |\Omega_b|e^{-i\phi_b} = \frac{\hat{\mu}_{42}\hat{e_b}E_b}{\hbar}e^{-i\phi_b}$, respectively, whereas $\hat{\mu}_{mn} = e\langle m|\hat{z}|n\rangle$ is the electronic dipole moment matrix element between the transition $|m\rangle \Leftrightarrow |n\rangle$, and the term $\phi_m (m = p, c, d, b)$ signifies the absolute phase of the applied field E_j. To investigate the light-matter interaction phenomena that are occurring in the ACQW system, we follow the density matrix formalism, which begins with the following equation:

$$\begin{aligned}\frac{\partial \rho_{ij}}{\partial t} = &-\frac{i}{\hbar}\sum_m (\hat{H}_{im}\rho_{mj} - \rho_{im}\hat{H}_{mj}) \\ &- \frac{1}{2}(\Gamma_{im}\rho_{mj} + \rho_{im}\Gamma_{mj}),\end{aligned} \tag{5}$$

where ρ_{ij} is the ijth matrix element. The first and second terms on the right side signify the coherent evolution of the state and radiative decay process within the system, respectively. Here, the electron population decay rate from a given energy level is incorporated in the equation through decay matrix Γ, which is defined as $\Gamma_{im} = \langle i|\Gamma|m\rangle = \gamma_i\delta_{im}$, where δ_{im} is the Kronecker δ. Adopting the procedure of Refs. [34,45], we obtain following Maxwell's Bloch equations for the density matrix elements:

$$\frac{\partial \tilde{\rho}_{11}}{\partial t} = i\Omega_p^*\tilde{\rho}_{41} - i\Omega_p\tilde{\rho}_{14}, \tag{6}$$

$$\frac{\partial \tilde{\rho}_{22}}{\partial t} = i\Omega_c^*\tilde{\rho}_{32} - i\Omega_c\tilde{\rho}_{23} + i\Omega_b^*\tilde{\rho}_{42} - i\Omega_b\tilde{\rho}_{24} - \gamma_2\tilde{\rho}_{22}, \tag{7}$$

$$\frac{\partial \tilde{\rho}_{33}}{\partial t} = i\Omega_c\tilde{\rho}_{23} - i\Omega_c^*\tilde{\rho}_{32} + i\Omega_d^*\tilde{\rho}_{43} - i\Omega_d\tilde{\rho}_{34} - \gamma_3\tilde{\rho}_{33}, \tag{8}$$

$$\begin{aligned}\frac{\partial \tilde{\rho}_{44}}{\partial t} = &i\Omega_p\tilde{\rho}_{14} - i\Omega_p^*\tilde{\rho}_{41} + i\Omega_b\tilde{\rho}_{24} - i\Omega_b^*\tilde{\rho}_{42} \\ &+ i\Omega_d\tilde{\rho}_{34} - i\Omega_d^*\tilde{\rho}_{43} - \gamma_4\tilde{\rho}_{44},\end{aligned} \tag{9}$$

$$\begin{aligned}\frac{\partial \tilde{\rho}_{21}}{\partial t} = &i\left(\Delta_p - \Delta_b + i\frac{\gamma_{21}}{2}\right)\tilde{\rho}_{21} + i\Omega_c^* e^{i\Phi}\tilde{\rho}_{31} \\ &+ i\Omega_b^*\tilde{\rho}_{41} - i\Omega_p\tilde{\rho}_{24},\end{aligned} \tag{10}$$

$$\begin{aligned}\frac{\partial \tilde{\rho}_{31}}{\partial t} = &i\left(\Delta_p - \Delta_d + i\frac{\gamma_{31}}{2}\right)\tilde{\rho}_{31} + i\Omega_c e^{-i\Phi}\tilde{\rho}_{21} \\ &+ i\Omega_d^*\tilde{\rho}_{41} - i\Omega_p\tilde{\rho}_{34},\end{aligned} \tag{11}$$

$$\begin{aligned}\frac{\partial \tilde{\rho}_{41}}{\partial t} = &i\left(\Delta_p + i\frac{\gamma_{41}}{2}\right)\tilde{\rho}_{41} + i\Omega_p(\tilde{\rho}_{11} - \tilde{\rho}_{44}) \\ &+ i\Omega_b\tilde{\rho}_{21} + i\Omega_d\tilde{\rho}_{31},\end{aligned} \tag{12}$$

$$\begin{aligned}\frac{\partial \tilde{\rho}_{32}}{\partial t} = &i\left(\Delta_c + i\frac{\gamma_{32}}{2}\right)\tilde{\rho}_{32} + i\Omega_c(\tilde{\rho}_{22} - \tilde{\rho}_{33}) \\ &+ i\Omega_d^* e^{i\Phi}\tilde{\rho}_{42} - i\Omega_b e^{i\Phi}\tilde{\rho}_{34},\end{aligned} \tag{13}$$

$$\begin{aligned}\frac{\partial \tilde{\rho}_{42}}{\partial t} = &i\left(\Delta_b + i\frac{\gamma_{42}}{2}\right)\tilde{\rho}_{42} + i\Omega_b(\tilde{\rho}_{22} - \tilde{\rho}_{44}) \\ &+ i\Omega_d e^{-i\Phi}\tilde{\rho}_{32} - i\Omega_c e^{-i\Phi}\tilde{\rho}_{43},\end{aligned} \tag{14}$$

$$\begin{aligned}\frac{\partial \tilde{\rho}_{43}}{\partial t} = &i\left(\Delta_d + i\frac{\gamma_{43}}{2}\right)\tilde{\rho}_{43} + i\Omega_d(\tilde{\rho}_{33} - \tilde{\rho}_{44}) \\ &+ i\Omega_p\tilde{\rho}_{13} + i\Omega_b e^{i\Phi}\tilde{\rho}_{23} - i\Omega_c^* e^{i\Phi}\tilde{\rho}_{42},\end{aligned} \tag{15}$$

where Δ_j $(j = p, c, d, b)$ is the detuning frequency of the corresponding applied field, which is defined as $\Delta_p = \omega_p - \frac{E_4-E_1}{\hbar}$, $\Delta_c = \omega_c - \frac{E_3-E_2}{\hbar}$, $\Delta_d = \omega_d - \frac{E_4-E_3}{\hbar}$, and $\Delta_b = \omega_b - \frac{E_4-E_2}{\hbar}$, respectively. The population conservation condition $\sum_{i=1}^{4}\tilde{\rho}_{ii} = 1$, together with $\rho_{mj} = \rho_{jm}^*(m, j = 1, 2, 3, 4; m \neq j)$, supplements the above equation. In order to derive the above equations, we have defined the relative phase of the applied fields in a close loop as $\Phi = \phi_c + \phi_d - \phi_b$, which is an important parameter that modifies the linear as well as nonlinear properties of the QW nanostructure. In addition, for the sake of simplicity, we assume that the angular frequency of the applied fields must satisfy the condition $\omega_c + \omega_d = \omega_b$, i.e., $\Delta_c + \Delta_d = \Delta_b$, which reduces to $k_c + k_d = k_b$. Moreover, we have used the following transformations: $\rho_{21} = \tilde{\rho}_{21}e^{i(\phi_b-\phi_p)}e^{-i(k_b z-\omega_b t)}e^{i(k_p z-\omega_p t)}$, $\rho_{31} = \tilde{\rho}_{31}e^{i(\phi_d-\phi_p)}e^{-i(k_d z-\omega_d t)}e^{i(k_p z-\omega_p t)}$, $\rho_{41} = \tilde{\rho}_{41}e^{-i\phi_p}e^{i(k_p z-\omega_p t)}$, $\rho_{42} = \tilde{\rho}_{42}e^{-i\phi_b}e^{i(k_b z-\omega_b t)}$, $\rho_{32} = \tilde{\rho}_{32}e^{-i\phi_c}e^{i(k_c z-\omega_c t)}$, and $\rho_{43} = \tilde{\rho}_{43}e^{-i\phi_d}e^{i(k_d z-\omega_d t)}$. In semiconductor QWs, $\gamma_{jl} = \gamma_j + \gamma_{jl}^{dph}(j = 2-4)$ signifies the total population decay rate from the energy subband $|j\rangle$, which consists of a population decay

rate due to inelastic LO phonon emission at low temperature and a dephasing term (γ_j^{dph}) originates not only from electron-electron and electron-phonon scattering, but also from inhomogeneous broadening due to scattering on interfaces.

In the steady state we assume that all the electrons will initially occupy the ground state, i.e., $\tilde{\rho}_{11} = 1$, $\tilde{\rho}_{ii}(i = 2, 3, 4) = 0$ at $t = 0$. Under the limit of a weak probe field approximation [12], we may also assume that the probe field is sufficiently weak in comparison to the control fields [i.e., $\Omega_p \ll \Omega_c$, Ω_d, and Ω_b]; under this assumption, the carrier in the ground state is not too much depleted [i.e., $\tilde{\rho}_{11} \simeq 1$, $\tilde{\rho}_{ii} \simeq 0$ $(i = 2, 3, 4)$, at $t > 0$]. Therefore we introduce the perturbative expansion $\tilde{\rho}_{ij} = \sum_k \tilde{\rho}_{ij}^{(k)}$, where $\tilde{\rho}_{ij}^{(k)}$ is the kth-order perturbation of $\tilde{\rho}_{ij}$. Within the regime of adiabatic formulation [44], it can be easily shown that $\tilde{\rho}_{ij}^{(0)} = \delta_{ij}(i \neq j)$, $\tilde{\rho}_{ii}^{(0)}(i = 2, 3, 4) \simeq 0$, and $\tilde{\rho}_{j1} \simeq \tilde{\rho}_{j1}^{(1)}\tilde{\rho}_{11}^{(0)}(j = 2, 3, 4)$. Note that $\tilde{\rho}_{ii}$ is the population density matrix element, while $\tilde{\rho}_{ij}$ is the optical response to the probe field for the transition $|i\rangle \rightarrow |j\rangle$. Therefore the population conservation condition is valid for the zeroth order in the perturbative expansion and not valid for higher-order terms, i.e., $\tilde{\rho}_{11}^{(0)} + \tilde{\rho}_{22}^{(0)} + \tilde{\rho}_{33}^{(0)} + \tilde{\rho}_{44}^{(0)} = 1$. By virtue of above approximations, Eqs. (10)–(12) reduce to

$$\frac{\partial \tilde{\rho}_{21}^{(1)}}{\partial t} = i\left(\Delta_p - \Delta_b + i\frac{\gamma_{21}}{2}\right)\tilde{\rho}_{21}^{(1)} + i\Omega_c^* e^{i\Phi}\tilde{\rho}_{31}^{(1)} + i\Omega_b^*\tilde{\rho}_{41}^{(1)} - i\Omega_p\tilde{\rho}_{24}^{(0)}, \tag{16}$$

$$\frac{\partial \tilde{\rho}_{31}^{(1)}}{\partial t} = i\left(\Delta_p - \Delta_d + i\frac{\gamma_{31}}{2}\right)\tilde{\rho}_{31}^{(1)} + i\Omega_c e^{-i\Phi}\tilde{\rho}_{21}^{(1)} + i\Omega_d^*\tilde{\rho}_{41}^{(1)} - i\Omega_p\tilde{\rho}_{34}^{(0)}, \tag{17}$$

$$\frac{\partial \tilde{\rho}_{41}^{(1)}}{\partial t} = i\left(\Delta_p + i\frac{\gamma_{41}}{2}\right)\tilde{\rho}_{41}^{(1)} + i\Omega_p\left(\tilde{\rho}_{11}^{(0)} - \tilde{\rho}_{44}^{(0)}\right) + i\Omega_b\tilde{\rho}_{21}^{(1)} + i\Omega_d\tilde{\rho}_{41}^{(1)}. \tag{18}$$

Considering only a linear response of the probe field (Ω_p) and introducing the Fourier transformation of Eqs. (16)–(18), we immediately obtain

$$\left(\omega + \Delta_p - \Delta_b + i\frac{\gamma_{21}}{2}\right)\beta_{21}^{(1)} + \Omega_c^* e^{i\Phi}\beta_{31}^{(1)} + \Omega_b^*\beta_{41}^{(1)} = 0, \tag{19}$$

$$\Omega_c e^{-i\Phi}\beta_{21}^{(1)} + \left(\omega + \Delta_p - \Delta_d + i\frac{\gamma_{31}}{2}\right)\beta_{31}^{(1)} + \Omega_d^*\beta_{41}^{(1)} = 0, \tag{20}$$

$$\Omega_b\beta_{21}^{(1)} + \Omega_d\beta_{31}^{(1)} + \left(\omega + \Delta_p + i\frac{\gamma_{41}}{2}\right)\beta_{41}^{(1)} = -\Lambda_p, \tag{21}$$

where $\beta_{ij}^{(1)}$ and Λ_p are, respectively, the Fourier transformation of $\tilde{\rho}_{ij}^{(1)}$ and Ω_p, and ω is the Fourier transformation variable. After some simple algebra, it is easy to obtain the following relations from Eqs. (19)–(21): $\beta_{21}^{(1)}(\omega) = \Lambda_p\frac{D_2(\omega,\Phi)}{D(\omega,\Phi)}$, $\beta_{31}^{(1)}(\omega) = \Lambda_p\frac{D_3(\omega,\Phi)}{D(\omega,\Phi)}$, and $\beta_{41}^{(1)}(\omega) = -\Lambda_p\frac{D_p(\omega)}{D(\omega,\Phi)}$. By virtue of the inverse Fourier transformation of $\beta_{21}^{(1)}(\omega)$, $\beta_{31}^{(1)}(\omega)$, and $\beta_{41}^{(1)}(\omega)$ we immediately obtain $\tilde{\rho}_{21}^{(1)}(0) = \Omega_p\frac{D_2(0,\Phi)}{D(0,\Phi)}$, $\tilde{\rho}_{31}^{(1)}(0) = \Omega_p\frac{D_3(0,\Phi)}{D(0,\Phi)}$, $\tilde{\rho}_{41}^{(1)}(0) = -\Omega_p\frac{D_p(0)}{D(0,\Phi)}$; where $D_p(\omega) = \{X(\omega)Y(\omega) - |\Omega_c|^2\}$, $D_2(\omega, \Phi) = \{Y(\omega)|\Omega_b| - |\Omega_c\Omega_d|e^{i\Phi}\}$, $D_3(\omega, \Phi) = \{X(\omega)|\Omega_d| - |\Omega_c\Omega_b|e^{-i\Phi}\}$, $D(\omega, \Phi) = \{X(\omega)Y(\omega)Z(\omega) - |\Omega_c|^2Z(\omega) - |\Omega_d|^2X(\omega) - |\Omega_b|^2Y(\omega) + 2\Omega_c\Omega_d\Omega_b\cos(\Phi)\}$, $X(\omega) = (\omega + \Delta_p - \Delta_b + i\frac{\gamma_{21}}{2})$, $Y(\omega) = (\omega + \Delta_p - \Delta_d + i\frac{\gamma_{31}}{2})$, and $Z(\omega) = (\omega + \Delta_p + i\frac{\gamma_{41}}{2})$.

Before proceeding to incorporate terms arising due to nonlinear polarization, we note an early work of nonlinear optical process using EIT by Harris *et al*. [46]. They have shown that by applying a coupling field between a metastable state and the upper state of an allowed transition to ground, one may obtain a resonantly enhanced third-order susceptibility while at the same time inducing transparency of the media. The susceptibility was calculated under the assumption that the Rabi frequency of the probe as well as the effective Rabi frequency of the signal between the ground and the metastable state are very small in comparison to the Rabi frequency of the control field. Under the above condition, the third-order nonlinear susceptibility was found to contain a term which is nonlinear just in the control beam. On the other hand, the nonlinear process, such as soliton propagation in atomic systems and quantum wells, has been extensively investigated by several workers using the probability amplitude as well as the density matrix formalism [47–49], where the nonlinear susceptibility has been derived using a slightly different procedure. In the present investigation, the probe beam is small, and to incorporate nonlinear polarization we adopt the procedure [47–49] that has been widely used in the investigation of nonlinear processes in atomic systems as well as in quantum wells. For simplicity we assume that the probe field is propagating along the z direction, and under the slowly varying envelope approximation (SVEA) [12], the equation for the propagating probe can be obtained from Maxwell's wave equations, which can be written as

$$\frac{\partial \Omega_p}{\partial z} + \frac{1}{c}\frac{\partial \Omega_p}{\partial t} = i\kappa\tilde{\rho}_{41}, \tag{22}$$

where $\kappa = \frac{N|\mu_{41}|^2}{2\hbar\epsilon_0 c}\omega_p$; c, ϵ_0, $\hbar$ are, respectively, the speed of the light in vacuum, the permittivity in free space, and Planck's constant. Here N is the carrier concentration in the semiconductor QW. Following [49] the density matrix element $\tilde{\rho}_{41}$ is evaluated (derivation shown in Appendix) as

$$\tilde{\rho}_{41} \simeq \left\{1 - \left(\left|\tilde{\rho}_{21}^{(1)}\right|^2 + \left|\tilde{\rho}_{31}^{(1)}\right|^2 + \left|\tilde{\rho}_{41}^{(1)}\right|^2\right) + \left(\left|\tilde{\rho}_{21}^{(1)}\right|^2 + \left|\tilde{\rho}_{31}^{(1)}\right|^2 + \left|\tilde{\rho}_{41}^{(1)}\right|^2\right)^2\right\}\tilde{\rho}_{41}^{(1)}. \tag{23}$$

Note that only those terms which lead to the Kerr nonlinearity have been retained and other higher-order terms neglected in Refs. [47–49], whereas, though small, we have retained terms up to $|\tilde{\rho}_{j1}^{(1)}|^4$, $j = 2, 3, 4$. The reason for retaining such small terms is based on the fact that occasionally even a small nonlinear term may be responsible for rich nonlinear dynamics. In view of the above, Eq. (22) is now rewritten as

$$\frac{\partial \Omega_p}{\partial z} + \frac{1}{c}\frac{\partial \Omega_p}{\partial t} = i\kappa\tilde{\rho}_{41}^{(1)} + (NLT)\tilde{\rho}_{41}^{(1)}, \tag{24}$$

where

$$NLT = -i\kappa\left\{\left(\left|\tilde{\rho}_{21}^{(1)}\right|^2 + \left|\tilde{\rho}_{31}^{(1)}\right|^2 + \left|\tilde{\rho}_{41}^{(1)}\right|^2\right) - \left(\left|\tilde{\rho}_{21}^{(1)}\right|^2 + \left|\tilde{\rho}_{31}^{(1)}\right|^2 + \left|\tilde{\rho}_{41}^{(1)}\right|^2\right)^2\right\}. \tag{25}$$

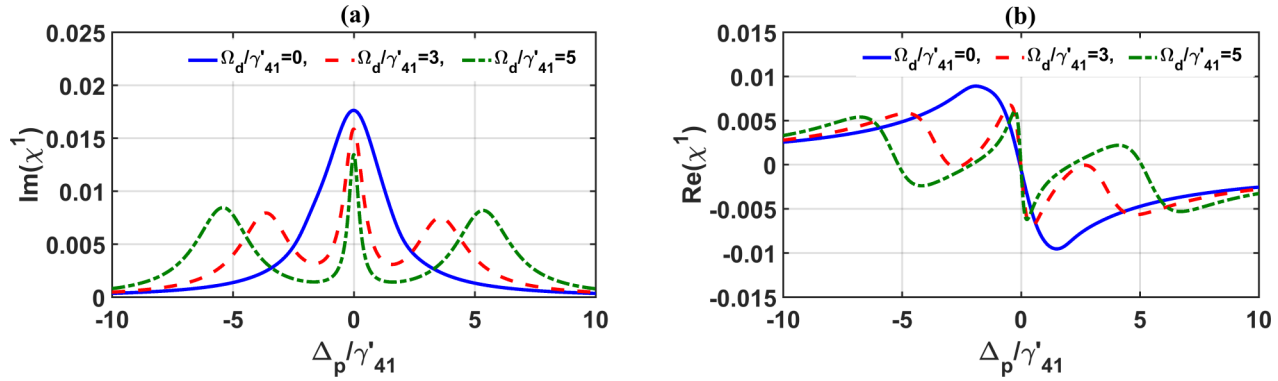

FIG. 2. Variations of the (a) imaginary and (b) real parts of linear susceptibility as a function of normalized probe detuning for different values of the Rabi frequency of the second control field (Ω_d), while the Rabi frequency of the first control field is fixed ($\Omega_c = 2\gamma'_{41}$) and Rabi frequency of the third control field is switched off, i.e., $\Omega_b = 0$. Other relevant parameters are $\Delta_d = \Delta_b = 0$, normalizing factor $\gamma'_{41} = 1$ ps^{-1}, and relative phase Φ of the applied fields is zero.

The total induced polarization $\vec{P}$ at the probe frequency ω_p is $\vec{P}(\omega_p) = \epsilon_0 \chi_p(\omega_p, \Phi)|E_p|$, where the susceptibility $\chi_p(\omega_p, \Phi)$ at the probe frequency ω_p can be written as the sum of linear and nonlinear terms as

$$\chi_p(\omega_p, \Phi) = \chi^{(1)}(\Phi) + \chi^{(3)}(\Phi)|E_p|^2 + \chi^{(5)}(\Phi)|E_p|^4 + \cdots . \tag{26}$$

Solving Eqs. (22)–(26), the analytical expressions of linear and higher-order nonlinear susceptibilities are obtained as

$$\chi^{(1)}(\Phi) = -\frac{2c\kappa}{\omega_p}\frac{D_p(0)}{D(0,\Phi)}, \tag{27}$$

$$\chi^{(3)}(\Phi) = \frac{2c\kappa}{\omega_p}\frac{|\mu_{41}|^2}{\hbar^2}\frac{D_p(0)}{D(0,\Phi)} \times \left\{\frac{|D_p(0)|^2 + |D_2(0,\Phi)|^2 + |D_3(0,\Phi)|^2}{|D(0,\Phi)|^2}\right\}, \tag{28}$$

$$\chi^{(5)}(\Phi) = -\frac{2c\kappa}{\omega_p}\frac{|\mu_{41}|^4}{\hbar^4}\frac{D_p(0)}{D(0,\Phi)} \times \left\{\frac{|D_p(0)|^2 + |D_2(0,\Phi)|^2 + |D_3(0,\Phi)|^2}{|D(0,\Phi)|^2}\right\}^2. \tag{29}$$

In the next section we analyze the properties of linear and nonlinear susceptibilities of the probe under the regime of EIT window in the QW system.

III. PROPERTIES OF PHASE CONTROL LINEAR AND NONLINEAR SUSCEPTIBILITIES

In this section we examine the behavior of the phase-dependent linear, Kerr, and quintic nonlinearities exhibited by the multiple ACQW system at the probe frequency. The value of several parameters related to the ACQW [40,50] are as follows: $N = 10^{20}$ m^{-3}, $\mu_{41} = 15.68 \times 10^{-29}$ C m, $\omega_p = 2.84 \times 10^{14}$ s^{-1}, thus $\kappa = 1.24 \times 10^{15}$ m^{-1} s^{-1}. The decay rates are $\gamma_{21} = 1.51 \times 10^{11}$ s^{-1}, $\gamma_{31} = \gamma_{41} = 3.03 \times 10^{12}$ s^{-1}, and the value of the normalization factor is chosen to be $\gamma'_{41} = 1$ ps^{-1}. Before proceeding further, we first examine the properties of the linear susceptibility ($\chi^{(1)}$) of the probe beam in absence of the relative phase (Φ) of the applied fields. In Fig. 2(a) we have depicted the variations of the imaginary part of the linear susceptibility with normalized probe detuning (Δ_p/γ'_{41}) for different values of the Rabi frequency (Ω_d) of the second control beam, while the Rabi frequency of the first control field is kept constant at $\Omega_c/\gamma'_{41} = 2$ and the third control field (Ω_b) is switched off. From Fig. 2(a), under the resonance (i.e., $\Delta_d = \Delta_b = 0$) it is evident that in absence of the second control beam (i.e., $\Omega_d = 0$), the probe beam experiences large absorption at around $\Delta_p = 0$. With the increase in the value of the Rabi frequency of the second control, the width of the absorption peak gradually reduces while side peaks emerges on both sides of the main peak. Consequently, transmission windows are created at the off-resonant positions ($\Delta_p \neq 0$) of the probe beam. The width of these two side windows increases with the increase in the value of Ω_d/γ'_{41}. Therefore, though the second control beam is not sufficient to create a transparency window at the probe resonance, secondary transmission windows can be created at the off-resonant positions. Figure 2(b) demonstrates the variation of the real part of $\chi^{(1)}$ versus normalized probe detuning (Δ_p/γ'_{41}) for different values of the Rabi frequency (Ω_d) of the second control beam, while the Rabi frequency of the first control field is kept constant at $\Omega_c/\gamma'_{41} = 2$, and the third control field (Ω_b) is switched off. As shown in Fig. 2(b), with the increase in the value of the second control beam Ω_d from 0 to $5\gamma'_{41}$, the slope of Re($\chi^{(1)}$) changes, and since this slope determines the group velocity of the beam, consequently, the group velocity can be controlled with the second control beam.

We now proceed to investigate the influence of the cyclic field (Ω_b) on the behavior of linear susceptibility. In Fig. 3 we have demonstrated the variations of the imaginary and real parts of $\chi^{(1)}$ with normalized probe detuning Δ_p/γ'_{41} for different values of the Rabi frequency of the third control beam (Ω_b), while values of the other two control fields have been kept constant at $\Omega_c/\gamma'_{41} = 2$ and $\Omega_d/\gamma'_{41} = 3$, respectively. From Fig. 3(a) we notice that with the application of finite value of the third control field, for example, for $\Omega_b/\gamma'_{41} = 2$, a transparency window is formed which

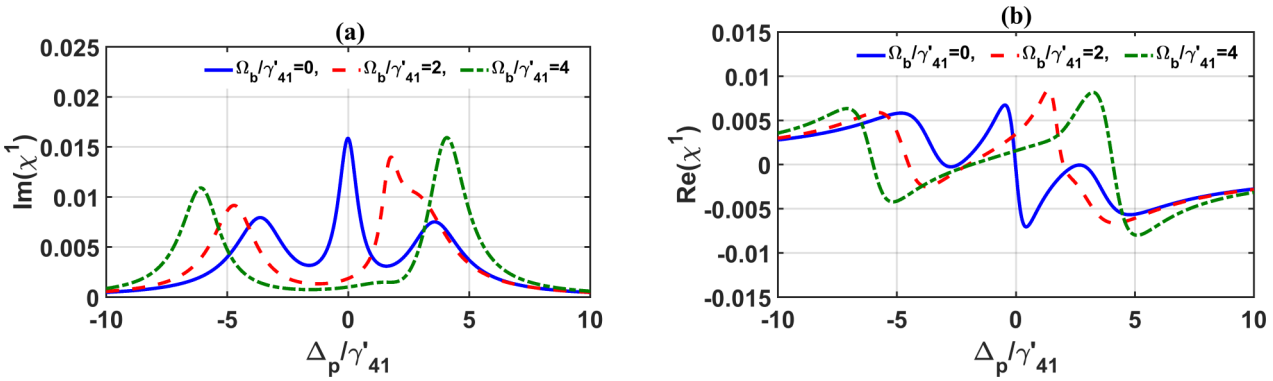

FIG. 3. Variations of the (a) imaginary and (b) real parts of linear susceptibility as a function of normalized probe detuning for different values of the Rabi frequency of the third control field (Ω_b), while the Rabi frequencies of the first and second control fields are fixed, i.e., $\Omega_c = 2\gamma'_{41}$ and $\Omega_d = 3\gamma'_{41}$. Other relevant parameters are $\Delta_d = \Delta_b = 0$, normalizing factor $\gamma'_{41} = 1$ ps^{-1}, and relative phase Φ of the applied fields is zero.

broadens further with increasing value of Ω_b. The suppression of the absorption of the probe beam is the manifestation of the quantum destructive interference effect which is governed by strong controlling beam, and the physical principle behind this is well understood and can be found elsewhere [7,8]. Meanwhile, from Fig. 3(b) we find that within the EIT window the slope of the real ($\chi^{(1)}$) changes from negative to positive in the domain $-4 \leqslant \Delta_p/\gamma'_{41} \leqslant 2$ for $\Omega_b/\gamma'_{41} = 2$, and similar behavior is observed for the case of $\Omega_b/\gamma'_{41} = 4$.

To this end we now examine the role of the relative phase Φ on the behavior of $\chi^{(1)}$. The variations of real and imaginary parts of $\chi^{(1)}$ with the probe detuning Δ_p/γ'_{41} for different values of relative phase have been demonstrated in Fig. 4. From figure it is evident that with the chosen values of Rabi frequencies and detuning a transmission window with negligible absorption over a broad detuning Δ_p appears when the phase $\Phi = 0$. With the increase in the value of Φ, the imaginary part of the refractive index does not change significantly within the probe detuning $-2.5\gamma'_{41} \leqslant \Delta_p \leqslant 2.5\gamma'_{41}$, except for the appearance of a small hump near $\Delta_p = 0$. Therefore, without much loss of accuracy, we can safely conclude the variation of Φ does not change the absorption property of the probe appreciably. However, a careful examination shows that the real part of the refractive index is susceptible to significant change due to the variation of Φ. Therefore dispersive properties of the probe beam can be controlled not only by the Rabi frequency of the control field but by the relative phase between them as well.

We now examine the effects of relative phase Φ on the properties of Kerr nonlinearity. The variations of the Kerr nonlinearity with probe detuning for different values of relative phase Φ have been depicted in Fig. 5, where the curves are drawn setting the control fields at resonance condition i.e., $\Delta_d = \Delta_b = 0$. These figures clearly indicate that the value of the Kerr nonlinearity can be varied by varying the relative phase as long as probe detuning $|\Delta_p/\gamma'_{41}| > 2.5$. For example, if we set $\Delta_p/\gamma'_{41} = 5$, then at $\Phi = 0$, $\chi^{(3)}$ possesses a positive value; however, at $\Phi = \frac{\pi}{2}$ the value of $\chi^{(3)}$ becomes negative, and at $\Phi = \pi$ the value still remains negative with decreasing magnitude and at $\Phi = \frac{3\pi}{2}$ the negative value further increase in magnitude. Therefore, with an appropriate choice of detunings of the control fields, the value and sign of the nonlinearity can be controlled by Φ. To have a better appreciation of the influence of Φ on $\chi^{(3)}$, we demonstrate the variations of $\chi^{(3)}$ with Φ at three different selected values of probe detuning Δ_p in Fig. 6. This figure clearly indicates that the magnitude and sign of the third-order susceptibility can be tuned as per requirement by suitably selecting the value of Φ. The sign of $\chi^{(3)}$ and the type of dispersion are a crucial factor for the creation of bright and dark solitons; therefore an appropriate condition for formation of solitons can be created by a suitable choice of Φ.

To this end, we now proceed to examine the behavior of the fifth-order nonlinearity $\chi^{(5)}$, which is popularly known as quintic nonlinearity. In order to investigate the influence of the relative phase on $\chi^{(5)}$, we have demonstrated the variations of Re($\chi^{(5)}$) with normalized detuning Δ_p/γ'_{41} for different values of Φ from 0 to 2π, while the Rabi frequencies of the three control fields have been kept constant at $\Omega_c/\gamma'_{41} = 2$, $\Omega_d/\gamma'_{41} = 3$, and $\Omega_b/\gamma'_{41} = 4$, respectively. From Fig. 7 it is amply clear that by varying the relative phase Φ, it is possible to control the amplitude of the fifth-order susceptibility. Note that usually the sign of Re($\chi^{(5)}$) is opposite to $\chi^{(3)}$. This behavior remains unaffected for all values of Φ. To have an idea about the magnitude of the quintic nonlinearity, we take a typical point in Fig. 7(d) and estimate its value. For example, at $\Delta_p/\gamma'_{41} = 0.75$, $\Omega_c/\gamma'_{41} = 2$, $\Omega_d/\gamma'_{41} = 3$, $\Omega_b/\gamma'_{41} = 4$, $\Delta_d = \Delta_b = 0$, and $\Phi = \frac{3\pi}{2}$, the typical value of $\chi^{(5)}$ is found to be -0.35×10^{-26} m^4/V^4, which is quite large in comparison to other nonlinear media. For example, a brief comparison is given in Table I, which shows that the present value of quintic nonlinearity is at least 12 orders larger in comparison to that of SiO_2 optical fibers. However, this value of the quintic nonlinearity could be controlled by suitably choosing

TABLE I. Comparison of the typical values of quintic nonlinearities in quantum wells and other media.

Materials	$\chi^{(5)}$ in m^4/V^4	References
As_2Se_3 glass	-1.29×10^{-39}	[51]
SiO_2 Fiber	-4.2×10^{-38}	[52]
$GaAs/Al_{0.33}Ga_{0.67}As$	-0.35×10^{-26}	Present work

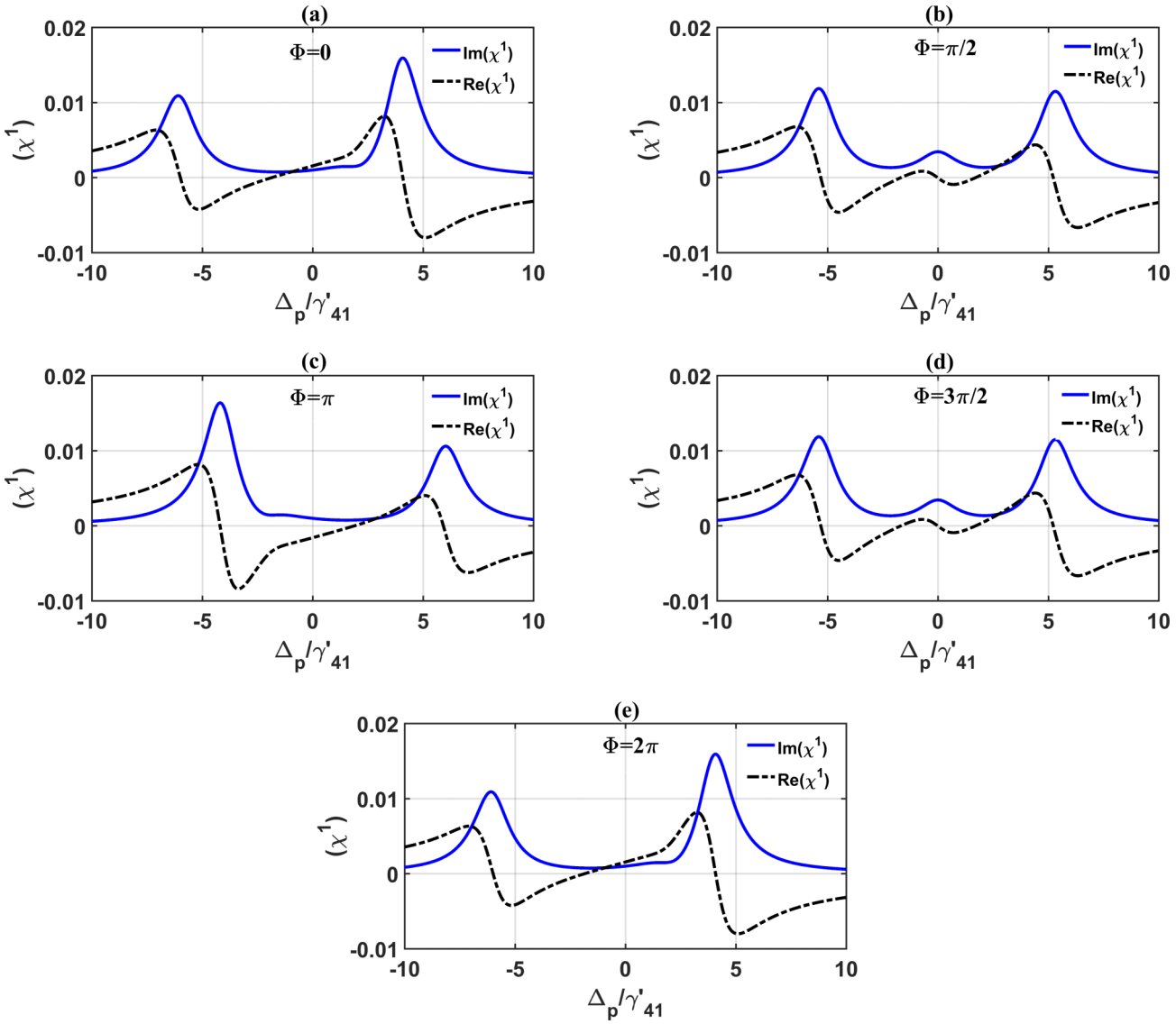

FIG. 4. Variations of the imaginary (solid line) and real parts (dashed-dot line) of linear susceptibility as a function of normalized probe detuning for different values of the relative phase Φ, while the Rabi frequencies of three control fields have been fixed at $\Omega_c = 2\gamma'_{41}$, $\Omega_d = 3\gamma'_{41}$, and $\Omega_b = 4\gamma'_{41}$, respectively. Here the value of detunings are $\Delta_d = \Delta_b = 0$, and the normalizing factor $\gamma'_{41} = 1\ \mathrm{ps}^{-1}$.

the Rabi frequencies of the control beam and relative phase factor between them.

IV. NONLINEAR SCHRÖDINGER EQUATION OF THE PROBE BEAM

In order to study the modulation instability of the probe beam, which could be either a continuous wave (CW) or a quasicontinuous wave (QCW), we need to derive an appropriate nonlinear Schrödinger equation. Therefore, as a first step, we perform the Fourier transformation of the linearized version of Eq. (24) to obtain

$$\frac{\partial \Lambda_p}{\partial z} - i\beta(\omega, \Phi)\Lambda_p = 0, \tag{30}$$

where the phase-dependent propagation constant of the probe field is defined as $\beta(\omega, \Phi) = \frac{\omega}{c} - \kappa \frac{D_p(\omega)}{D(\omega,\Phi)}$. The analytical solution of Eq. (30) can be readily obtained as

$$\Lambda_p(z, \omega) = \Lambda_p(0, \omega)e^{i\beta(\omega,\Phi)z}. \tag{31}$$

The propagation constant $\beta(\omega, \Phi)$ in Eq. (31) is a function of frequency ω and phase Φ. It is the linear dispersion relation of the probe field with central angular frequency ω_p. The propagation constant $\beta(\omega, \Phi)$ can be expanded into a rapidly converging power series around the central frequency ω_p of the probe field, which corresponds to $\omega = 0$. Note that an identical procedure has been widely used in the literature [12,13,20]:

$$\beta(\omega, \Phi) = \beta(0, \Phi) + \beta_1(0, \Phi)\omega + \beta_2(0, \Phi)\frac{\omega^2}{2} + \beta_3(0, \Phi)\frac{\omega^3}{6} + \beta_4(0, \Phi)\frac{\omega^4}{24} + \cdots, \tag{32}$$

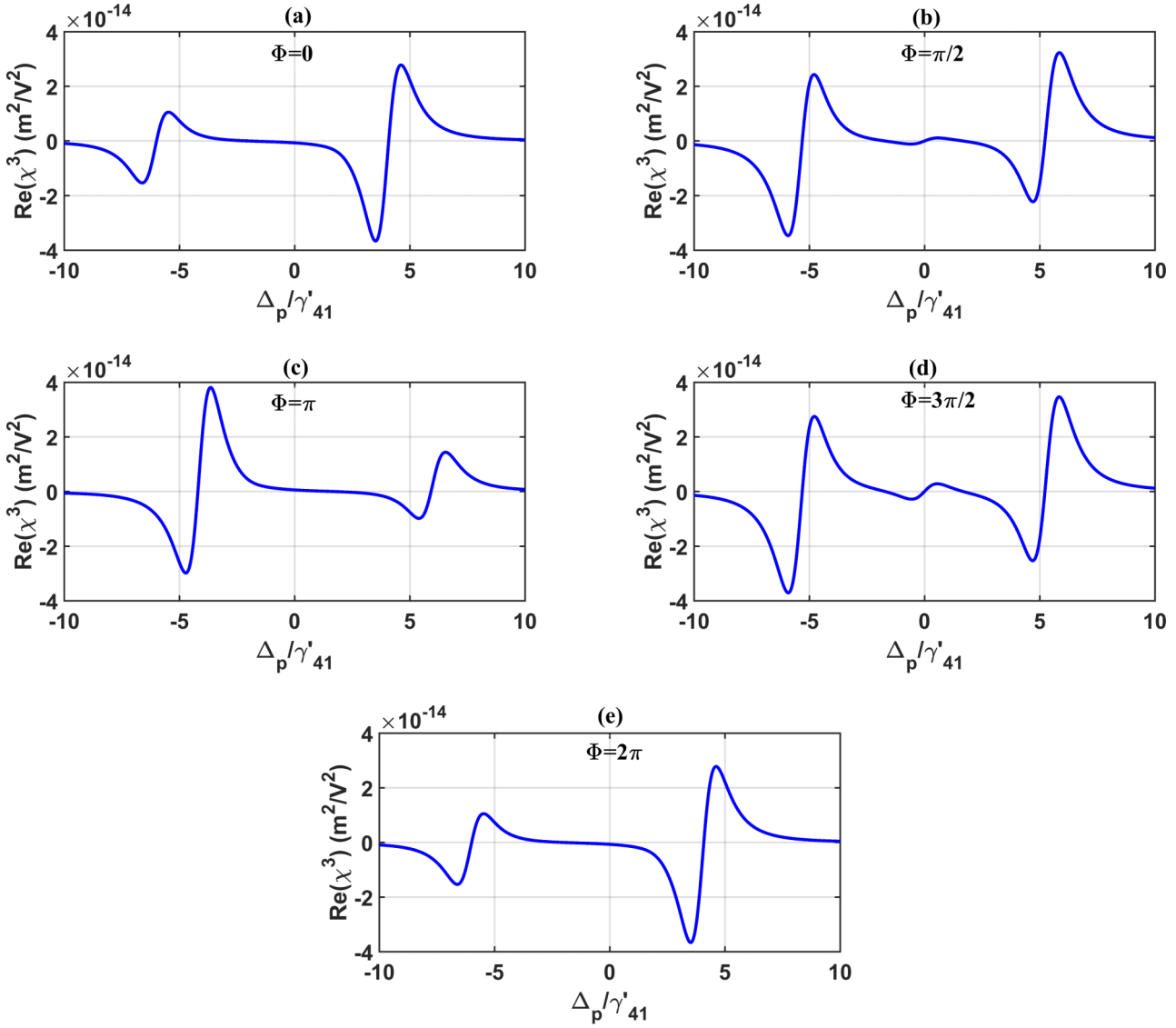

FIG. 5. Variations of the real part of the third-order susceptibility $[(\chi^{(3)})]$ as a function of normalized probe detuning (Δ_p) for different values of the relative phase Φ, while the Rabi frequencies of three control fields have been fixed at $\Omega_c = 2\gamma'_{41}$, $\Omega_d = 3\gamma'_{41}$, and $\Omega_b = 4\gamma'_{41}$, respectively. Here the values of detunings are $\Delta_d = \Delta_b = 0$, and the normalizing factor $\gamma'_{41} = 1$ ps^{-1}.

where $\beta_n(\omega, \Phi) = \frac{d^n\beta(\omega,\Phi)}{d\omega^n}|_{\omega=0}$ and $\beta(0, \Phi) = \phi + i\frac{\alpha}{2}$, and ϕ and α are the phase shift per unit length and linear absorption of the probe beam, respectively. $\beta_1(0, \Phi)$ is related to the group velocity $v_g[= \mathrm{Re}(1/\beta_1(0, \Phi))]$ of the probe field, and $\beta_2(0, \Phi)$ represents the group velocity dispersion (GVD) of the probe. Likewise, $\beta_3(0, \Phi)$ and $\beta_4(0, \Phi)$ are respectively the third- and fourth-order dispersion terms. The mathematical expressions of $\beta(0, \Phi)$, $\beta_1(0, \Phi)$, $\beta_2(0, \Phi)$, $\beta_3(0, \Phi)$, and $\beta_4(0, \Phi)$ are as follows:

$$\beta(0, \Phi) = -\kappa \frac{D_p(0)}{D(0, \Phi)}, \tag{33}$$

$$\beta_1(0, \phi) = \frac{1}{c} - \kappa \frac{D_{12}(0)}{[D(0, \Phi)]^2} + \kappa \frac{D_p(0)D_{11}(0)}{[D(0, \Phi)]^2}, \tag{34}$$

$$\beta_2(0, \Phi) = -\frac{2\kappa}{D(0, \Phi)} + 2\kappa \frac{D_{12}(0)D_{11}(0)}{[D(0, \Phi)]^2} + \kappa \frac{D_p(0)D_{21}(0)}{[D(0, \Phi)]^2} - \kappa \frac{2D_p(0)[D_{11}(0)]^2}{[D(0, \Phi)]^3}, \tag{35}$$

$$\beta_3(0, \Phi) = 6\kappa \frac{D_{11}(0)}{[D(0, \Phi)]^2} - 6\kappa \frac{D_{12}(0)[D_{11}(0)]^2}{[D(0, \Phi)]^3} + 3\kappa \frac{D_{12}(0)D_{21}(0)}{[D(0, \Phi)]^2} - 6\kappa \frac{D_p(0)D_{21}(0)D_{11}(0)}{[D(0, \Phi)]^3} + 6\kappa \frac{D_p(0)}{[D(0, \Phi)]^2} + 6\kappa \frac{D_p(0)[D_{11}(0)]^3}{[D(0, \Phi)]^4}, \tag{36}$$

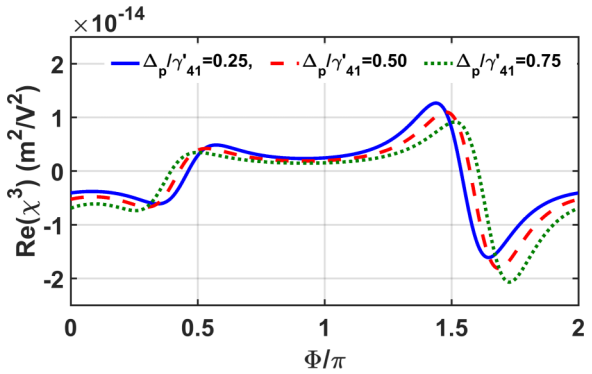

FIG. 6. Variation of the real part of the third-order susceptibility ($\chi^{(3)}$) as a function of the relative phase Φ between the applied fields for different values of the probe detuning (Δ_p), while the Rabi frequencies of the three control fields have been fixed at $\Omega_c = 2\gamma'_{41}$, $\Omega_d = 3\gamma'_{41}$, and $\Omega_b = 4\gamma'_{41}$, respectively. Here the values of detunings are $\Delta_d = \Delta_b = 0$, and the normalizing factor $\gamma'_{41} = 1$ ps^{-1}.

$$\beta_4(0,\Phi) = -24\kappa\frac{[D_{11}(0)]^2}{[D(0,\Phi)]^3} - 48\kappa\frac{D_p(0)D_{11}(0)}{[D(0,\Phi)]^3} + 24\kappa\frac{D_{12}(0)[D_{11}(0)]^3}{[D(0,\Phi)]^4} + 24\kappa\frac{D_{12}(0)}{[D(0,\Phi)]^2} - 6\kappa\frac{D_{12}(0)D_{11}(0)D_{21}(0)}{[D(0,\Phi)]^3} - 6\kappa\frac{[D_{11}(0)]^4}{[D(0,\Phi)]^5} + 12\kappa\frac{D_{21}(0)}{[D(0,\Phi)]^2} - 6\kappa\frac{D_p(0)[D_{21}(0)]^2}{[D(0,\Phi)]^3} + 36\kappa\frac{D_p(0)D_{21}(0)[D_{11}(0)]^2}{[D(0,\Phi)]^4}, \quad (37)$$

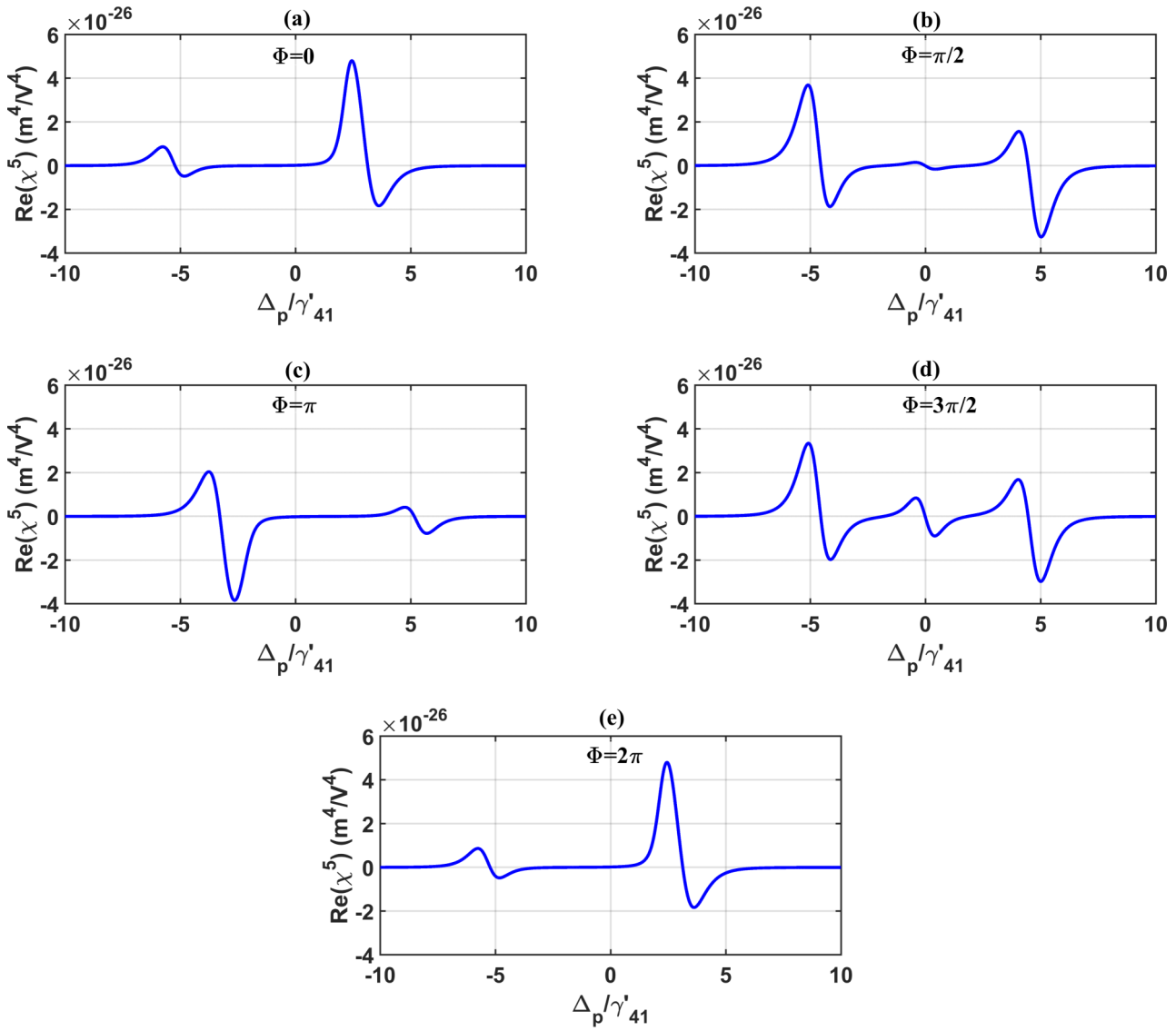

FIG. 7. Variations of the real part of the fifth-order susceptibility Re($\chi^{(5)}$) as a function of normalized probe detuning (Δ_p) for different values of the relative phase Φ, while the Rabi frequencies of three control fields have been fixed at $\Omega_c = 2\gamma'_{41}$, $\Omega_d = 3\gamma'_{41}$, and $\Omega_b = 4\gamma'_{41}$, respectively. Here the values of detunings are $\Delta_d = \Delta_b = 0$, and the normalizing factor $\gamma'_{41} = 1$ ps^{-1}.

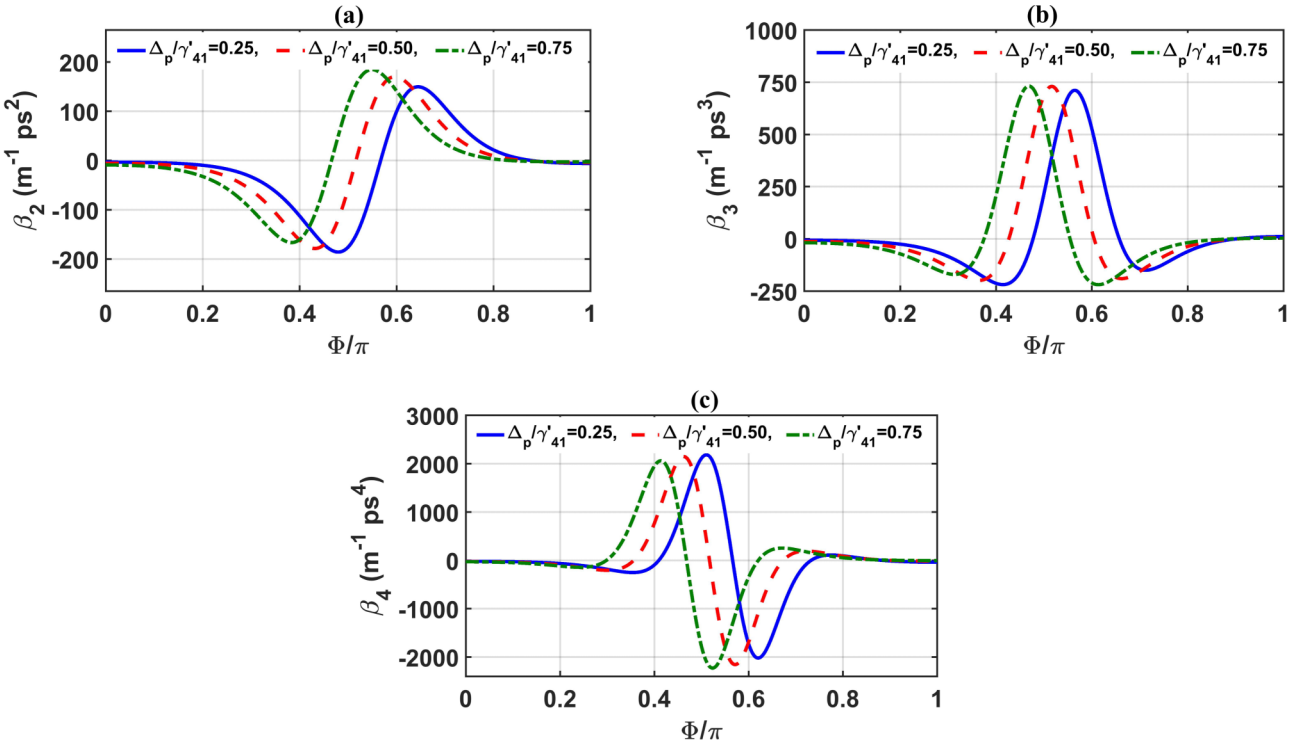

FIG. 8. Variations of (a) second-order (β_2), (b) third-order (β_3), and (c) fourth-order (β_4) dispersion parameters as a function of relative phase between the applied fields for three different values of probe detuning (Δ_p/γ'_{41}), while the Rabi frequencies of three control fields have been fixed at $\Omega_c = 2\gamma'_{41}$, $\Omega_d = 3\gamma'_{41}$, and $\Omega_b = 4\gamma'_{41}$, respectively. Here the values of detunings are $\Delta_d = 0.5\gamma'_{41}$, $\Delta_b = 0.25\gamma'_{41}$, and normalizing factor $\gamma'_{41} = 1$ ps^{-1}.

where

$$D_{11}(\omega) = \{Y(\omega)Z(\omega) + Z(\omega)X(\omega) + X(\omega)Y(\omega) - |\Omega_c|^2 - |\Omega_d|^2 - |\Omega_b|^2\}, \tag{38}$$

$$D_{12}(\omega) = \left(2\omega + 2\Delta_p - \Delta_d - \Delta_b + i\frac{\gamma_{21}}{2} + i\frac{\gamma_{31}}{2}\right), \tag{39}$$

and

$$D_{21}(\omega) = (6\omega + 6\Delta_p - 2\Delta_b - 2\Delta_d + i\gamma_{21}i\gamma_{31} + i\gamma_{41}). \tag{40}$$

To examine the influence of the relative phase Φ on dispersion properties, we have demonstrated the variations of β_2, β_3, and β_4 with the relative phase Φ for three different values of the probe detuning in Fig. 8. Note that all three dispersion terms change with the change in the values of Φ. It should be pointed out that Eq. (30) is obtained using only the linear response of the probe beam by ignoring nonlinearity associated with this system. In order to investigate nonlinear evolution of the probe beam, we need to incorporate appropriate nonlinear terms in the propagation equation. These higher-order nonlinear terms are responsible for various interesting phenomena, such as self-phase modulation (SPM), cross-phase modulation (XPM), modulation instability (MI), soliton propagation, supercontinuum generation (SC), etc. Therefore, to proceed further, we take the nonlinear version of Eq. (30) and rewrite it as

$$\frac{\partial \Lambda_p}{\partial z} - i\beta(\omega, \Phi)\Lambda_p - (NLT)\tilde{\rho}_{41}^{(1)} = 0. \tag{41}$$

By virtue of Eqs. (25), (31), and (32), the above equation reduces to

$$\left\{\frac{\partial}{\partial z} + i\beta_1(0,\Phi)\omega - i\beta_2(0,\Phi)\frac{\omega^2}{2} + i\beta_3(0,\Phi)\frac{\omega^3}{6} + \beta_4(0,\Phi)\frac{\omega^4}{24}\right\}\Lambda_p(0,\omega)e^{i\beta(0,\Phi)z}$$
$$= i\kappa\frac{D_p(\omega)}{D(\omega,\Phi)}\Lambda_p(0,\omega)e^{i\beta(0,\Phi)z}\left\{\left(\left|\tilde{\rho}_{21}^{(1)}\right|^2 + \left|\tilde{\rho}_{31}^{(1)}\right|^2 + \left|\tilde{\rho}_{41}^{(1)}\right|^2\right) - \left(\left|\tilde{\rho}_{21}^{(1)}\right|^2 + \left|\tilde{\rho}_{31}^{(1)}\right|^2 + \left|\tilde{\rho}_{41}^{(1)}\right|^2\right)^2\right\}. \tag{42}$$

Here we have taken terms up to ω^4 in the expansion of $\beta(\omega, \Phi)$. By virtue of the substitution of expressions of $\tilde{\rho}_{21}^{(1)}$, $\tilde{\rho}_{31}^{(1)}$, and $\tilde{\rho}_{41}^{(1)}$, and the inverse Fourier transformation of Eq. (42), we immediately obtain

$$i\frac{\partial\Omega_p}{\partial z} + i\beta_1(0,\Phi)\frac{\partial\Omega_p}{\partial t} - \frac{\beta_2(0,\Phi)}{2}\frac{\partial^2\Omega_p}{\partial t^2} - i\frac{\beta_3(0,\Phi)}{6}\frac{\partial^3\Omega_p}{\partial t^3} + \frac{1}{24}\beta_4(0,\Phi)\frac{\partial^4\Omega_p}{\partial t^4} + \frac{\omega_p\hbar^2}{2c|\mu_{41}|^2}\chi^{(3)}(\Phi)|\Omega_p|^2\Omega_p e^{-\alpha z}$$
$$+ \frac{\omega_p\hbar^4}{2c|\mu_{41}|^4}\chi^{(5)}(\Phi)|\Omega_p|^4\Omega_p e^{-2\alpha z} = 0. \tag{43}$$

Introducing the moving frame $\xi = z$ and $T = t - z\beta_1(0, \Phi)$, Eq. (43) can be recast in the following form:

$$i\frac{\partial A}{\partial \xi} - \frac{1}{2}\beta_2(0,\Phi)\frac{\partial^2 A}{\partial T^2} - \frac{i}{6}\beta_3(0,\Phi)\frac{\partial^3 A}{\partial T^3} + \frac{1}{24}\beta_4(0,\Phi)\frac{\partial^4 A}{\partial T^4} + \gamma(\Phi)|A|^2 A e^{-\alpha\xi} + \delta(\Phi)|A|^4 A e^{-2\alpha\xi} = 0, \tag{44}$$

where $A = \frac{\hbar\Omega_p}{\mu_{41}}(\frac{n_0 c\epsilon_0 S}{2})^{\frac{1}{2}}$ is the normalized envelope of the probe beam. $\gamma(\Phi) = \frac{\omega_p}{n_0 c^2 \epsilon_0 S}\chi^{(3)}(\Phi)$ and $\delta(\Phi) = \frac{2\omega_p}{n_0^2 c^3 \epsilon_0^2 S^2}\chi^{(5)}(\Phi)$ are respectively the phase-dependent Kerr and quintic nonlinear coefficients. Here n_0 and S are respectively the linear refractive index and cross section area of the probe beam. Equation (44) represents the modified form of nonlinear Schrödinger equation which describes the evolution of the CW or quasi-CW probe beam in coupled QW systems. Since further investigation has been carried out within the EIT window where the absorption of the probe beam is sufficiently weak, i.e., $\alpha \approx 0$, therefore without loss of generality we can set $e^{-\alpha\xi} \approx e^{-2\alpha\xi} \approx 1$.

V. MODULATION INSTABILITY OF THE PROBE BEAM

In this section we now proceed to investigate the modulation instability of the CW or QCW probe field [25,53]. The steady-state solution of Eq. (44) can be written as

$$A(\xi, T) = \sqrt{P_0}e^{i\{\gamma(\Phi)P_0 + \delta(\Phi)P_0^2\}\xi}. \tag{45}$$

To examine whether the continuous wave (CW) probe beam is stable under small perturbation, we introduce a small perturbation in the following form:

$$A(\xi, T) = \{\sqrt{P_0} + a(\xi, T)\}e^{i\{\gamma(\Phi)P_0 + \delta(\Phi)P_0^2\}\xi}, \tag{46}$$

where $|a(\xi, T)| \ll \sqrt{P_0}$. Here $\sqrt{P_0}$ and $a(\xi, T)$ are respectively the amplitudes of the CW probe beam in the steady state and small perturbation. Therefore the steady state becomes unstable if the perturbation grows exponentially. The substitution of Eq. (46) in Eq. (44) and subsequent linearization leads to the following equation for the perturbation $a(\xi, T)$:

$$i\frac{\partial a}{\partial \xi} - \frac{\beta_2(0,\Phi)}{2}\frac{\partial^2 a}{\partial T^2} - \frac{i}{6}\beta_3(0,\Phi)\frac{\partial^3 a}{\partial T^3} + \frac{1}{24}\beta_4(0,\Phi)\frac{\partial^4 a}{\partial T^4} + \{\gamma(\Phi)P_0 + 2\delta(\Phi)P_0^2\}(a + a^*) = 0. \tag{47}$$

We assume the following ansatz for the perturbation $a(\xi, T)$:

$$a(\xi, T) = Ce^{i(K\xi - \Omega T)} + De^{-i(K\xi - \Omega T)}, \tag{48}$$

where C and D represent the amplitude of small perturbation; K and Ω are complex wave number and modulation frequencies, respectively. The use of Eq. (48) in Eq. (47) yields two homogeneous equations of C and D, which are as follows:

$$C(-K + G) + \{\gamma(\Phi)P_0 + 2\delta(\Phi)P_0^2\}D = 0, \tag{49}$$

$$\{\gamma(\Phi)P_0 + 2\delta(\Phi)P_0^2\}C + (K + \tilde{G})D = 0, \tag{50}$$

where $G = [\beta_2(0,\Phi)\frac{\Omega^2}{2} + \beta_3(0,\Phi)\frac{\Omega^3}{6} + \beta_4(0,\Phi)\frac{\Omega^4}{24} + \{\gamma(\Phi)P_0 + 2\delta(\Phi)P_0^2\}]$ and $\tilde{G} = [\beta_2(0,\Phi)\frac{\Omega^2}{2} - \beta_3(0,\Phi)\frac{\Omega^3}{6} + \beta_4(0,\Phi)\frac{\Omega^4}{24} + \{\gamma(\Phi)P_0 + 2\delta(\Phi)P_0^2\}]$. The nontrivial solution of Eqs. (49) and (50) leads to the following dispersion relation:

$$K = \frac{1}{6}\beta_3(0,\Phi)\Omega^3 \pm \left\{\left\{\beta_2(0,\Phi)\Omega^2 + \beta_4(0,\Phi)\frac{\Omega^4}{24}\right\} \times \{\gamma(\Phi)P_0 + 2\delta(\Phi)P_0^2\} - \left\{\beta_2(0,\Phi)\frac{\Omega^2}{2} + \beta_4(0,\Phi)\frac{\Omega^4}{24}\right\}^2\right\}^{\frac{1}{2}}. \tag{51}$$

The gain $g(\Omega)$ of the instability at perturbed frequency Ω is obtained as

$$g(\Omega) = 2\mathrm{Im}(K) = 2\left\{\left[\beta_2(0,\Phi)\Omega^2 + \beta_4(0,\Phi)\frac{\Omega^4}{24}\right] \times \left[\gamma(\Phi)P_0 + 2\delta(\Phi)P_0^2\right] - \left[\beta_2(0,\Phi)\frac{\Omega^2}{2} + \beta_4(0,\Phi)\frac{\Omega^4}{24}\right]^2\right\}^{\frac{1}{2}}, \tag{52}$$

where $\mathrm{Im}(K)$ signifies the imaginary part of the wave number K. The maximum gain of the instability is obtained at $\Omega = \Omega_m$, which turns out to be

$$\Omega_m = \pm\left[\left\{6\left[\left\{\left(\frac{\beta_2(0,\Phi)}{\beta_4(0,\Phi)}\right)^2 + \frac{2}{3}\frac{\gamma(\Phi)P_0 + 2\delta(\Phi)P_0^2}{\beta_4(0,\Phi)}\right\}^{\frac{1}{2}} - 6\frac{\beta_2(0,\Phi)}{\beta_4(0,\Phi)}\right\}^{\frac{1}{2}}\right]. \tag{53}$$

We first examine the growth of the modulation instability in the absence of the fourth-order dispersion, i.e., we set $\beta_4 = 0$ in the beginning. For simplicity we fix the value of the Rabi frequency of three control fields at $\Omega_c = 2\gamma'_{41}$, $\Omega_d = 3\gamma'_{41}$, and $\Omega_b = 4\gamma'_{41}$, respectively. The probe and control field detunings are chosen as $\Delta_p = 0.75\gamma'_{41}$, $\Delta_d = 0.5\gamma'_{41}$, and $\Delta_b = 0.25\gamma'_{41}$. In Fig. 9 we have demonstrated the variations of MI gain as a function of perturbation frequency for different values of relative phase Φ. The curves in the left panel represent MI dynamics in the absence of quintic nonlinearity, while the curves in the right panel represent the MI dynamics in the presence of quintic nonlinearity. One common characteristic of these

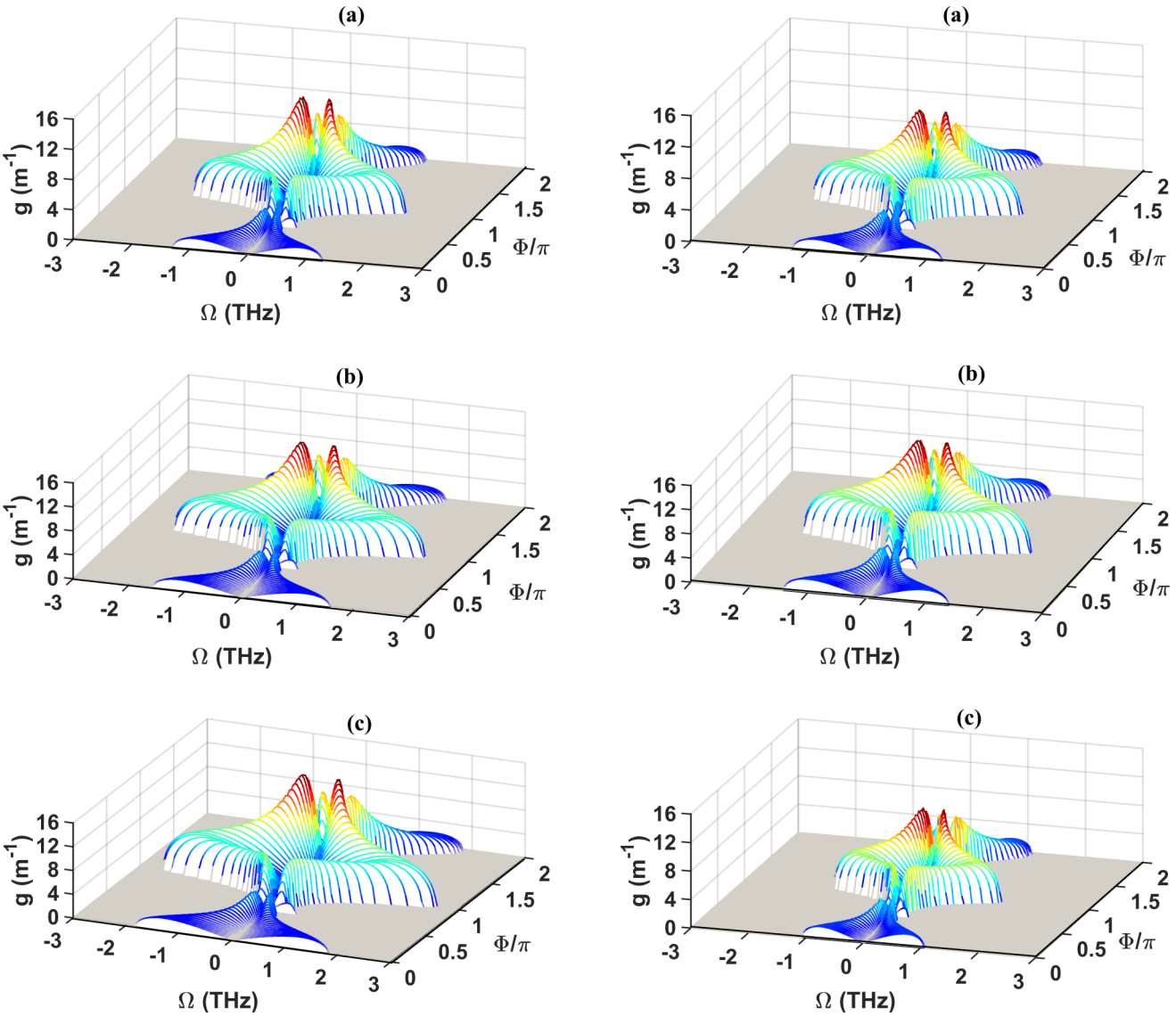

FIG. 9. Variations of MI gain with the perturbed frequency and relative phase Φ for different values of pump peak power P_0: (a) $P_0 =$ 50 mW, (b) $P_0 = 75$ mW, and (c) $P_0 = 100$ mW. In the left panel only Kerr nonlinearity is present, while in the right panels both Kerr and quintic nonlinearities are present. Here in all the subplots $\beta_4 = 0$, detuning frequencies are $\Delta_p = 0.75\gamma'_{41}$, $\Delta_d = 0.5\gamma'_{41}$, $\Delta_b = 0.25\gamma'_{41}$, and the Rabi frequencies of three control fields have been fixed at $\Omega_c = 2\gamma'_{41}$, $\Omega_d = 3\gamma'_{41}$, and $\Omega_b = 4\gamma'_{41}$, respectively.

curves is evident immediately, i.e., the incredible influences of the relative phase on the gain of the instability. For example, in the left panel of Fig. 9(a), the gain of the instability as well as the bandwidth of unstable frequencies gradually decrease with the increase in the value of relative phase Φ from zero to $\frac{\pi}{2}$, and the gain of the instability disappears at $\Phi = \frac{\pi}{2}$. However, the instability gain reappears for $\Phi > \frac{\pi}{2}$, and both the instability gain and the bandwidth increase with the increase in the value of Φ until it reaches a value π, beyond which once again the gain and the bandwidth decrease with the increase in Φ and finally disappear at $\Phi = \frac{3\pi}{2}$. The gain of the instability again reappears for $\Phi > \frac{3\pi}{2}$. Both the instability gain and the bandwidth of unstable frequencies vary periodically with a period of $\Phi = 2\pi$. An important feature of the instability is that the instability could be completely suppressed by a suitable choice of Φ. On the other hand, the system could be made more susceptible to the modulation instability by an appropriate choice of the value of phase Φ. For example, the largest unstable frequency bandwidth is achievable at $\Phi = \pi$. Therefore Φ is an important parameter which could control the growth of the instability. Another feature, which is usual in optical systems, is the increase of the growth of the instability as well as the bandwidth of unstable frequencies with the increase in power of the probe beam when the instability is driven by the Kerr nonlinearity alone.

We now examine the role of quintic nonlinearity on the instability gain using the right panel of Fig. 9. The qualitative behavior of the variation of instability gain and bandwidth of unstable frequencies with Φ is similar to the previous case of Kerr-driven instability. However, the variation of instability dynamics with power in the present case is different due to the saturating nature of the quintic nonlinearity. The quintic nonlinearity becomes appreciable only at high power. For example, at a low power of $P_0 = 50$ mW, the instability

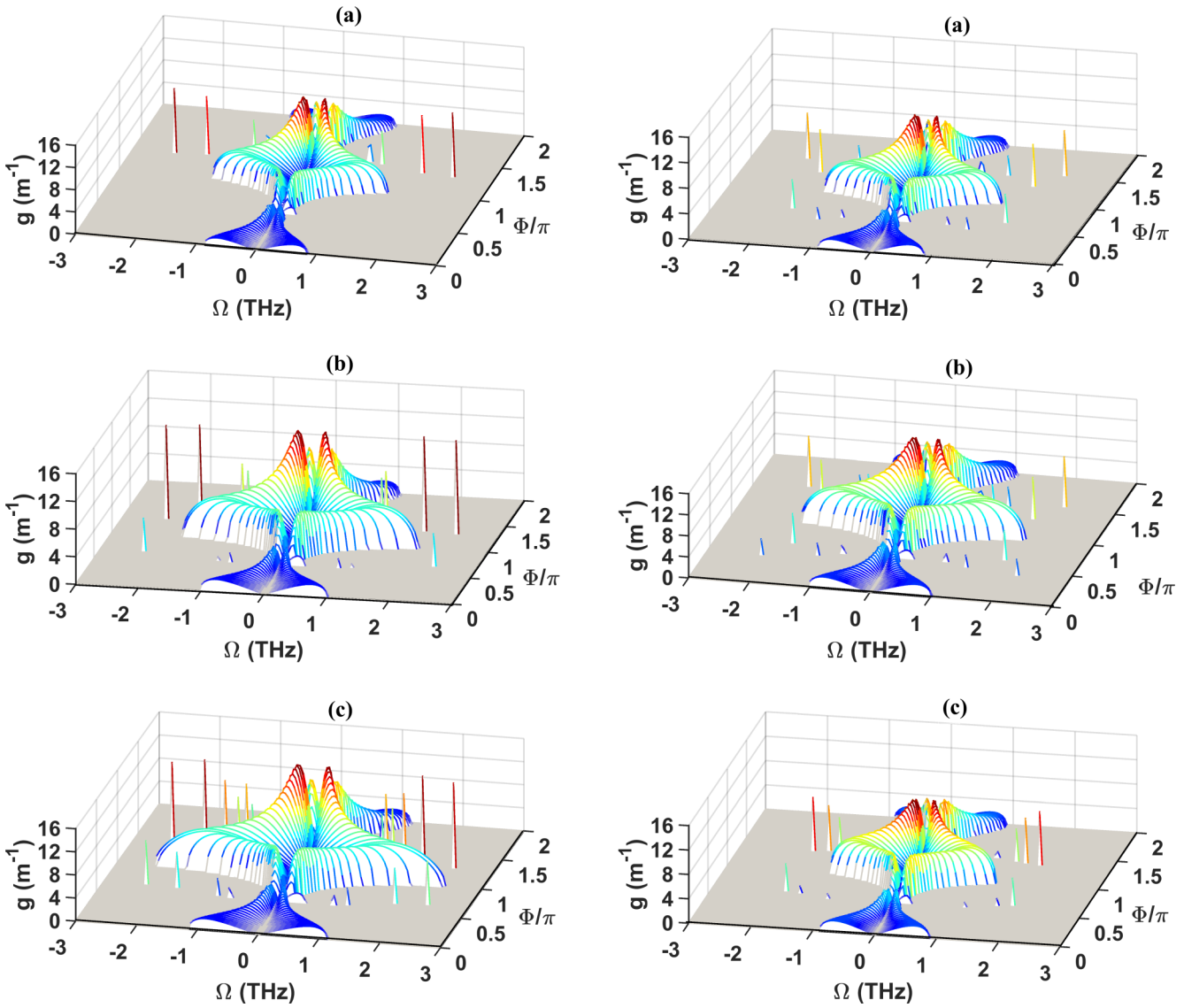

FIG. 10. Variations of MI gain with the perturbed frequency and relative phase Φ for different values of pump peak power P_0: (a) $P_0 =$ 50 mW, (b) $P_0 = 75$ mW, and (c) $P_0 = 100$ mW. In the left panel only Kerr nonlinearity is present, while in the right panels both Kerr and quintic nonlinearities are present. Here in all the subplots $\beta_4 \neq 0$, detuning frequencies are $\Delta_p = 0.75\gamma'_{41}$, $\Delta_d = 0.5\gamma'_{41}$, $\Delta_b = 0.25\gamma'_{41}$, and the Rabi frequencies of three control fields have been fixed at $\Omega_c = 2\gamma'_{41}$, $\Omega_d = 3\gamma'_{41}$, and $\Omega_b = 4\gamma'_{41}$, respectively.

dynamics is identical to that of Kerr-driven instability in terms of quality and quantity. However, at a power of $P_0 = 100$ mW, though the qualitative behavior remains unaffected, the magnitude of the growth and the bandwidth decrease appreciably with the increase in power of the probe beam.

To this end we investigate the instability dynamics in the presence of fourth-order dispersion β_4. The variations of the instability gain as a function of perturbed frequency and relative phase between electromagnetic fields for different values of probe power are depicted in Fig. 10. The left and right panel of the figure respectively represent the dynamics of the MI in the absence and presence of quintic nonlinearity. The qualitative behavior of the growth of the instability is very similar to the previous case as depicted in Fig. 9 and is explained in the previous paragraph with two notable differences. The first one is the reduction in bandwidth of unstable frequencies and magnitude of the gain. The second one is more interesting, the appearance of discrete sidebands at certain values of Φ. In order to have a better appreciation of the growth dynamics, in Fig. 11 we have displayed the variations of instability gain using the contour plots. Note that secondary discrete sidebands appear as dots in all six subplots.

At this stage it shall be worthy to investigate the role of probe detuning on the instability dynamics. Figure 12 illustrates the variations of MI gain as a function of the perturbed frequency and relative phase for four different values of probe detuning. Without any loss of generality, we ignore the quintic nonlinearity and only consider finite β_4. For illustration of the effect of probe detuning on the instability, we have taken four different values, i.e., (a) $\frac{\Delta_p}{\gamma'_{41}} = 0$, (b) $\frac{\Delta_p}{\gamma'_{41}} = 0.25$, (c) $\frac{\Delta_p}{\gamma'_{41}} = 0.50$, and (d) $\frac{\Delta_p}{\gamma'_{41}} = 0.75$. From Fig. 12(a) it is evident that the structure of the growth dynamics is very rich for zero probe detuning ($\Delta_p/\gamma'_{41} = 0$). Initially, at $\Phi/\pi = 0$

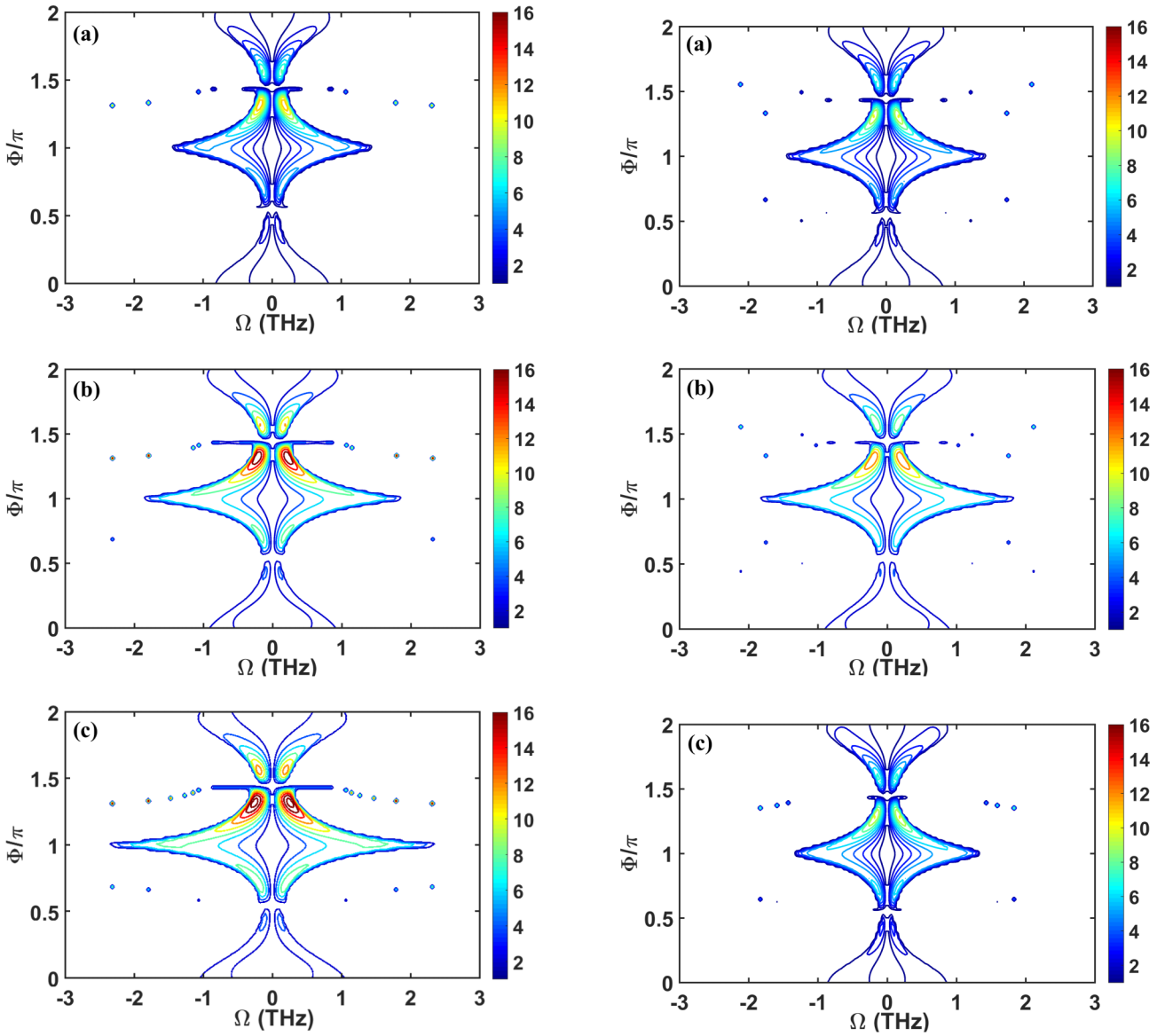

FIG. 11. Contour plots of MI gain with the perturbed frequency and relative phase Φ for different values of pump peak power P_0: (a) $P_0 =$ 50 mW, (b) $P_0 = 75$ mW, and (c) $P_0 = 100$ mW. In the left panel only Kerr nonlinearity is present, while in the right panel both Kerr and quintic nonlinearities are present. Here, in all the subplots $\beta_4 \neq 0$, detuning frequencies are $\Delta_p = 0.75\gamma'_{41}$, $\Delta_d = 0.5\gamma'_{41}$, $\Delta_b = 0.25\gamma'_{41}$, and the Rabi frequencies of three control fields have been fixed at $\Omega_c = 2\gamma'_{41}$, $\Omega_d = 3\gamma'_{41}$, and $\Omega_b = 4\gamma'_{41}$, respectively.

the unstable frequencies appear within $\Omega = 1$–2 THz. With the increase in the value of Φ, the unstable band of frequencies gradually decreases and shifts towards lower values, and finally the instability disappears near $\Phi/\pi = 0.5$. The instability resurfaces for $\Phi/\pi > 0.5$, and one can notice the occasional appearance of sideband spikes near Φ/π close to 0.6. The unstable band of frequencies increases with the value of Φ from 0.6, and a discrete sideband appears when Φ/π is close to 1. For values of $\Phi/\pi > 1$, the discrete sideband appears and a band of unstable frequencies decreases for further increase of Φ. Again, several sideband spikes appear when the value of Φ/π is close to 1.5, and once again the instability disappears near $\Phi/\pi = 1.5$. We now shift our attention to the instability growth for probe detuning ($\Delta_p/\gamma'_{41} = 0.25$). Three important differences from the previous case could be noticed. The first one, unlike the previous case, initially at $\Phi/\pi =$ 0 the unstable frequencies appear within $\Omega = 0$–1.7 THz. The second one is, overall, the bandwidth in the unstable frequencies is smaller in comparison to the previous case. The third one is the disappearance of sidebands near $\Phi/\pi = 1$. At a larger probe detuning of $\Delta_p/\gamma'_{41} = 0.5$, the behavior of the MI gain is identical to the case when $\Delta_p/\gamma'_{41} = 0.25$. A further increase in the value of Δ_p/γ'_{41} to 0.75, however, reduces the bandwidth of the gain when $0 < \Phi/\pi < 1.0$ and increases the bandwidth of the gain when $1 < \Phi/\pi < 1.5$. In addition, several discrete sidebands in the region of $1.0 < \Phi/\pi < 2.0$ disappear. Before closing, note the results of an important investigation by Kang *et al*. [54] on light switching at low light levels based on quantum interference in a four-level atomic system. The experiment was done using cold Rb atoms confined in a magneto-optical trap. They have demonstrated the phase control interference between three-photon

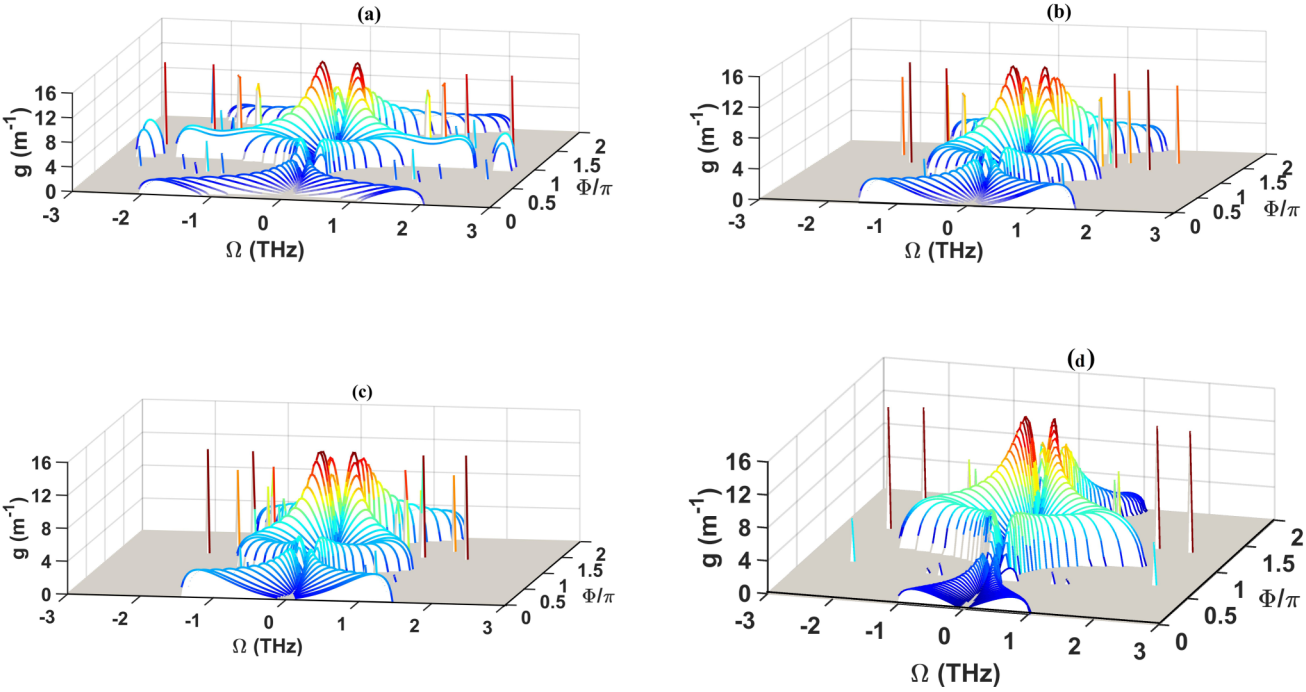

FIG. 12. Variations of the MI gain with the perturbed frequency and relative phase Φ for different values of normalized probe detuning (Δ_p/γ'_{41}): (a) $\Delta_p/\gamma'_{41} = 0$, (b) $\Delta_p/\gamma'_{41} = 0.25$, (c) $\Delta_p/\gamma'_{41} = 0.50$, and (d) $\Delta_p/\gamma'_{41} = 0.75$. Here, in all the subplots $\beta_4 \neq 0$, $\delta = 0$, detuning frequencies are $\Delta_d = 0.5\gamma'_{41}$, $\Delta_b = 0.25\gamma'_{41}$, probe power is fixed at $P_0 = 75$ mW, and the Rabi frequencies of three control fields have been fixed at $\Omega_c = 2\gamma'_{41}$, $\Omega_d = 3\gamma'_{41}$, and $\Omega_b = 4\gamma'_{41}$, respectively.

and one-photon excitation and the resulting phase switching of light absorption and/or transmission at very low light powers ($<10^{-7}$ W). It was observed that one weak control field can be used to control another weak probe field and vice versa at ultralow light levels. The phase control interference could be implemented near single-photon levels, and the four-level system may be used as an absorptive quantum switch which turns on and off single-probe photons by single-control photons at different frequencies. On the other hand, though the present ACQW also possesses four energy levels, the theoretical premise of the present study covers a different range of phenomena. For example, Kang *et al*. did not observe the modulation instability of the probe or the control beam in their experiment, which was performed with the probe and control beam power levels $<10^{-7}$ W (the intensity ~ 0.1 mW/cm^2). At this power level one would not expect modulation instability since the threshold of this instability is much higher, which is predicted in the present investigation.

VI. CONCLUSION

In summary, we have examined the phase-dependent dispersive and optical nonlinear properties of asymmetrically coupled quantum well systems under the regime of electromagnetically induced transparency. It is shown that though the relative phase Φ has marginal influence over the electromagnetically induced transparency window, it has significant influence on the behavior of the real part of the linear susceptibility and, hence, dispersive properties of the system. In addition, the system exhibits very large Kerr and quintic nonlinearities, which could be also controlled by controlling the relative phase between the applied electromagnetic fields. We have shown that a propagating continuous or quasicontinuous probe undergoes modulation instability whose dynamics is primarily governed by the relative phase between the applied electromagnetic fields. The gain and bandwidth of unstable frequencies of the MI could be controlled by the relative phase. An important feature of the MI is that by a suitable choice of the phase, the instability could be completely suppressed; on the other hand, by appropriate choice of the value of phase the system could be made more susceptible to the modulation instability as well. Both the fourth-order dispersion and quintic nonlinearity considerably reduce the growth and bandwidth of unstable frequencies. In addition, the fourth-order dispersion plays an important role in the creation of discrete sidebands.

ACKNOWLEDGMENTS

We thank the anonymous reviewers for insightful comments which have been very helpful in improving the quality of the manuscript. This work is financially supported by the Deference Research Devolopment Organization (DRDO), New Delhi, Government of India, through Grant No. ERIP/ER/1202225/M/01/1668. R.M. would like to thank DRDO for providing a fellowship.

APPENDIX

The derivation of the nonlinear term is based on the method adopted in Ref. [49]. By virtue of the normalization condition,

the density matrix elements obey

$$\mathrm{Tr}(\tilde{\rho}) = \tilde{\rho}_{11} + \tilde{\rho}_{22} + \tilde{\rho}_{33} + \tilde{\rho}_{44} = 1. \tag{A1}$$

It is well known that the probability amplitude and density matrix formalisms yield identical expressions of susceptibility in any physical system. Therefore we define the density matrix elements in terms of probability amplitudes [55] and write the density matrix element $\tilde{\rho}_{nm}$ as

$$\tilde{\rho}_{nm} = C_m^* C_n, \tag{A2}$$

where C_n is the probability amplitude of finding the electron in the eigenstate $|n>$. By virtue of (A2), Eq. (A1) is rewritten as

$$|C_1|^2 + |C_2|^2 + |C_3|^2 + |C_4|^2 = 1. \tag{A3}$$

We use the approximations

$$\tilde{\rho}_{11} \simeq 1 \quad \text{and} \quad \tilde{\rho}_{ii} \simeq 0 \quad (i = 2, 3, 4). \tag{A4}$$

In view of (A2), $\tilde{\rho}_{11} = |C_1|^2$ and $|C_1|^2 \simeq 1$, since $\tilde{\rho}_{11} \simeq 1$.

We now introduce the perturbation expansion

$$\tilde{\rho}_{ij} = \sum_k \tilde{\rho}_{ij}^{(k)} = \tilde{\rho}_{ij}^{(0)} + \tilde{\rho}_{ij}^{(1)} + \tilde{\rho}_{ij}^{(2)} + \cdots, \tag{A5}$$

$$\tilde{\rho}_{ij}^{(0)} = 0 \ (i \neq j), \quad \tilde{\rho}_{ii}^{(0)} = 0 \ (i = 2, 3, 4), \quad \tilde{\rho}_{11} \simeq \tilde{\rho}_{11}^{(0)} \simeq 1. \tag{A6}$$

Therefore the probe coherence term $\tilde{\rho}_{41}$ can be written as

$$\begin{aligned}
&\tilde{\rho}_{41} \simeq \tilde{\rho}_{41}^{(1)}\big(1 \simeq \tilde{\rho}_{41}^{(1)}\big)|C_1|^2, \quad \text{since} \quad |C_1|^2 \simeq 1 \\
&\tilde{\rho}_{41} \simeq \tilde{\rho}_{41}^{(1)}\{1 - (|C_2|^2 + |C_3|^2 + |C_4|^2)\}, \\
&\simeq \tilde{\rho}_{41}^{(1)}\{1 - (|C_2|^2 + |C_3|^2 + |C_4|^2)|C_1|^2\}, \\
&\simeq \tilde{\rho}_{41}^{(1)}[1 - (|C_2|^2 + |C_3|^2 + |C_4|^2)\{1 - (|C_2|^2 + |C_3|^2 \\
&\quad + |C_4|^2)\}], \\
&\simeq \tilde{\rho}_{41}^{(1)}[1 - (|C_2|^2 + |C_3|^2 + |C_4|^2) + (|C_2|^2 + |C_3|^2 \\
&\quad + |C_4|^2)^2].
\end{aligned} \tag{A7}$$

From Eq. (A2) we can write

$$\begin{aligned}
&\tilde{\rho}_{21} = C_1^* C_2, \quad \tilde{\rho}_{31} = C_1^* C_3, \ \tilde{\rho}_{41} = C_1^* C_4, \\
&|\tilde{\rho}_{21}|^2 = (C_1^* C_2)(C_2^* C_1) = |C_2|^2 |C_1|^2 \simeq |C_2|^2, \\
&|\tilde{\rho}_{31}|^2 = (C_1^* C_3)(C_3^* C_1) = |C_3|^2 |C_1|^2 \simeq |C_3|^2, \\
&|\tilde{\rho}_{41}|^2 = (C_1^* C_4)(C_4^* C_1) = |C_4|^2 |C_1|^2 \simeq |C_4|^2.
\end{aligned}$$

Inserting the above in Eq. (A7) yields

$$\begin{aligned}
\tilde{\rho}_{41} \simeq \tilde{\rho}_{41}^{(1)}\{1 &- (|\tilde{\rho}_{21}|^2 + |\tilde{\rho}_{31}|^2 + |\tilde{\rho}_{41}|^2) \\
&+ (|\tilde{\rho}_{21}|^2 + |\tilde{\rho}_{31}|^2 + |\tilde{\rho}_{41}|^2)^2\}.
\end{aligned} \tag{A8}$$

By retaining only up to first-order terms in the perturbation expansion, we get

$$\begin{aligned}
\tilde{\rho}_{21} &= \tilde{\rho}_{21}^{(0)} + \tilde{\rho}_{21}^{(1)} = \tilde{\rho}_{21}^{(1)}, \\
\tilde{\rho}_{31} &= \tilde{\rho}_{31}^{(0)} + \tilde{\rho}_{31}^{(1)} = \tilde{\rho}_{31}^{(1)}, \\
\tilde{\rho}_{41} &= \tilde{\rho}_{41}^{(0)} + \tilde{\rho}_{41}^{(1)} = \tilde{\rho}_{41}^{(1)},
\end{aligned}$$

since $\tilde{\rho}_{ij}^{(0)} = 0$ from Eq. (A6). Therefore Eq. (A8) can be rewritten as

$$\begin{aligned}
\tilde{\rho}_{41} \simeq \tilde{\rho}_{41}^{(1)}\big\{1 &- \big(|\tilde{\rho}_{21}^{(1)}|^2 + |\tilde{\rho}_{31}^{(1)}|^2 + |\tilde{\rho}_{41}^{(1)}|^2\big) \\
&+ \big(|\tilde{\rho}_{21}^{(1)}|^2 + |\tilde{\rho}_{31}^{(1)}|^2 + |\tilde{\rho}_{41}^{(1)}|^2\big)^2\big\}.
\end{aligned} \tag{A9}$$

[1] C. Hang, Y. Li, L. Ma, and G. Huang, Phys. Rev. A **74**, 012319 (2006).
[2] J.-H. Wu, J.-Y. Gao, J.-H. Xu, L. Silvestri, M. Artoni, G. C. La Rocca, and F. Bassani, Phys. Rev. Lett. **95**, 057401 (2005).
[3] H. Kang, G. Hernandez, and Y. Zhu, Phys. Rev. Lett. **93**, 073601 (2004).
[4] D. Felinto, D. Moretti, R. A. de Oliveira, and J. W. R. Tabosa, Opt. Lett. **35**, 3937 (2010).
[5] M. D. Frogley, J. F. Dynes, M. Beck, J. Faist, and C. C. Philips, Nat. Mater. **5**, 175 (2006).
[6] J. F. Dynes, M. D. Frogley, J. Rodger, and C. C. Phillips, Phys. Rev. B **72**, 085323 (2005).
[7] J. P. Marangos, J. Mod. Opt. **45**, 471 (1998).
[8] M. Fleischhauer, A. Imamoglu, and J. P. Marangos, Rev. Mod. Phys. **77**, 633 (2005).
[9] Y. Niu, S. Gong, R. Li, Z. Xu, and X. Liang, Opt. Lett. **30**, 3371 (2005).
[10] A. Joshi and M. Xiao, Appl. Phys. B **79**, 65 (2004).
[11] T. K. Paraiso, M. Wouters, Y. Leger, F. Morier-Genoud, and B. Deveaud-Pledran, Nat. Mater. **9**, 655 (2010).
[12] W. X. Yang, J. M. Hou, and R. K. Lee, Phys. Rev. A **77**, 033838 (2008).
[13] C. Zhu and G. Huang, Phys. Rev. B **80**, 235408 (2009).
[14] S. Shwetanshumala, S. Konar, and A. Biswas, Appl. Phys. B **111**, 53 (2013).
[15] J. Li, J. Liu, and X. Yang, Superlattices Microstruct. **44**, 166 (2008).
[16] Y. Wu, J. Saldana, and Y. Zhu, Phys. Rev. A **67**, 013811 (2003).
[17] X. X. Yang, Z.-W. Li, and Y. Wu, Phys. Lett. A **340**, 320 (2005).
[18] N. Borgohain, M. Belic, and S. Konar, Ann. Phys. **361**, 107 (2015).
[19] C. Zhu and G. Huang, Opt. Exp. **19**, 23364 (2011).
[20] C. Hang and G. Huang, Opt. Exp. **18**, 2952 (2010).
[21] H. Sun, S. Gong, Y. Niu, S. Jin, R. Li, and Z. Xu, Phys. Rev. B **74**, 155314 (2006).
[22] S. Konar, S. Jana, and M. Mishra, Opt. Commun. **255**, 114 (2005).
[23] W. X. Wang, T. T. Zha, and R. K. Lee, Phys. Lett. A **374**, 355 (2009).
[24] N. Borgohain, M. Belic, and S. Konar, J. Opt. **18**, 115001 (2016).
[25] N. Borgohain and S. Konar, J. Appl. Phys. **119**, 213103 (2016).
[26] A. F. Terzis, S. G. Kosionis, J. Boviatsis, and E. Paspalakis, J. Mod. Opt. **63**, 451 (2015).

[27] Y. Peng, A. Yang, B. Chen, Y. Xu, and X. Hu, J. Opt. Soc. Am. B **31**, 2188 (2014).
[28] R. Mukherjee and S. Konar, Results Phys. **17**, 103090 (2020).
[29] M. S. Zubairy, A. B. Matsko, and M. O. Scully, Phys. Rev. A **65**, 043804 (2002).
[30] D. K. Giri and P. S. Gupta, Opt. Commun. **221**, 135 (2003).
[31] Y. Zhang, U. Khadka, B. Anderson, and M. Xiao, Phys. Rev. Lett. **102**, 013601 (2009).
[32] J. A. Greenberg and D. J. Gauthier, Europhys. Lett. **98**, 24001 (2012).
[33] G. Fibnich, N. Gavish, and X. P. Wang, Physica D **231**, 55 (2007).
[34] J. F. Dynes and E. Paspalakis, Phys. Rev. B **73**, 233305 (2006).
[35] A. Joshi, Phys. Rev. B **79**, 115315 (2009).
[36] M. Sahrai, M. Momeni-Demne, and J. Poursamad, J. Opt. Soc. Am. B **32**, 1139 (2015).
[37] J. Wang and H. Fan, J. Lumin. **130**, 2084 (2010).
[38] H. R. Hamedi and G. Juzeliunas, Phys. Rev. A **91**, 053823 (2015).
[39] K. T. Kapale and M. S. Zubairy, Phys. Rev. A **73**, 023813 (2006).
[40] J. Faist, C. Sirtori, F. Cappaso, L. Pfeiffer, and K. W. West, Appl. Phys. Lett. **64**, 872 (1994).
[41] G. Bastard, Phys. Rev. B **24**, 5693 (1981); D. F. Nelson, R. C. Miller, and D. A. Kleinman, *ibid.* **35**, 7770 (1987).
[42] Z. Wang, Y. Zhang, E. Paspalakis, and B. Yu, Phys. Rev. A **102**, 063509 (2020).
[43] X. Hao, W.-X. Yang, X. Lu, J. Liu, P. Huang, C. Ding, and X. Yang, Phys. Lett. A **372**, 7081 (2008).
[44] M. O. Scually and M. S. Zubairy, *Quantum Optics* (Cambridge University Press, Cambridge, England, 2001).
[45] M. Sahrai, H. Tajalli, K. T. Kapale, and M. Suhail Zubairy, Phys. Rev. A **70**, 023813 (2004).
[46] S. E. Harris, J. E. Field, and A. Imamoglu, Phys. Rev. Lett. **64**, 1107 (1990).
[47] Y. Wu and L. Deng, Phys. Rev. Lett. **93**, 143904 (2004).
[48] Y. Wu and L. Deng, Opt. Lett. **29**, 2064 (2004).
[49] W. X. Yang, J. M. Hou, Y. Y. Lin, and R. K. Lee, Phys. Rev. A **79**, 033825 (2009).
[50] X. Hao, C. Ding, X.-Y. Lü, J. Li, and X. Yang, Physica E **42**, 1984 (2010).
[51] G. Boudebs, S. Cherukulappurath, H. Leblond, J. Troles, F. Smektala, and F. Sanchez, Opt. Commun. **219**, 427 (2003).
[52] D. Pushkarov and S. Tanev, Opt. Commun. **124**, 354 (1996).
[53] A. Choudhuri and K. Porsezian, Phys. Rev. A **85**, 033820 (2012).
[54] H. Kang, G. Hernandez, J. Zhang, and Y. Zhu, Phys. Rev. A **73**, 011802(R) (2006).
[55] R. W. Boyd, *Nonlinear Optics* (Academic Press, New York, 2008).